Multifunctional fire-resistant and flame-triggered shape memory epoxy nanocomposites containing carbon dots

Chemical Engineering Journal 484 (2024) 149327

Contents lists available at ScienceDirect

Chemical Engineering Journal

journal homepage: www.elsevier.com/locate/cej

Multifunctional fire-resistant and flame-triggered shape memory epoxy nanocomposites containing carbon dots

Aurelio Bifulco [a,*], Claudio Imparato [a], Immacolata Climaco [a], Daniele Battegazzore [b], Michele Perrella [a], Giuseppe Vitiello [a,c], Antonio Aronne [a], Giulio Malucelli [b]

[a] Department of Chemical, Materials and Production Engineering (DICMaPI), University of Naples Federico II, P.le Tecchio 80, 80125 Naples, Italy
[b] Department of Applied Science and Technology, Politecnico di Torino, Viale Teresa Michel 5, 15121 Alessandria, Italy
[c] CSGI, Center for Colloid and Surface Science, Via della Lastruccia 3, 50019 Sesto Fiorentino, Florence, Italy

ARTICLE INFO

Keywords:
Epoxy resin nanocomposites
Epoxy coatings
Carbon dots
Shape recovery
Hydrophobic surface
Fire resistance

ABSTRACT

Carbon quantum dots (CDs) are widely used as semiconductor systems, due to their facile synthesis and optical characteristics. CDs have been employed to enhance the light emission, UV resistance, and anticorrosive performances of epoxy nanocomposites (ENCs). Herein, we investigated the use of CDs to prepare multifunctional cycloaliphatic ENCs showing shape recovery capability. Following a waste-to-wealth approach, CDs were obtained from humic acid by a hydrothermal route. ENCs containing CDs exhibited photoluminescence, while the simultaneous addition of CDs and hexadecyltrimethoxysilane accounted for heat/flame-triggered shape recovery capability and hydrophobicity (contact angles as high as 137°). The polar character of silane-functionalized CDs allowed for their segregation at the surface of ENCs, making them very fire resistant. In particular, the CDs exerted an outstanding thermal shielding effect on the surface of ENCs, lowering the heat transfer at the boundary layer and increasing the time to flaming combustion up to ~ 76 %. Besides, the graphitic nature of CDs and their charring behavior led to a huge increase in the back temperature at the ignition point (up to ~ 30 %) during burn-through tests. Notwithstanding the low loadings (not exceeding 0.3 wt%) of CDs, ENCs lost their structural integrity only after almost 1 min of blowpipe flame application to their surface, whereas the resin counterpart degraded in less than 20 s. Besides, cone calorimetry tests carried out on ENCs highlighted a significant reduction of total smoke release (up to ~ 40 %) compared to unfilled epoxy. Finally, we demonstrated the possibility of using multifunctional ENCs containing CDs as unique identification technology for polypropylene packaging, opening new perspectives on the effective protection of genuine products from counterfeiting.

1. Introduction

Owing to their excellent properties, epoxy resins are widely employed in several industrial applications, such as electronic and electrical equipment, coating, packaging, painting, and adhesive bonding [1,2]. This class of polymers accounts for ~ 70 % of the global thermoset market, with a compound annual growth rate of around 6.46 % by 2024 [3,4]. The final properties of epoxy resins are strongly dependent on the selected curing conditions, employed monomer, and curing agent. For example, the use of an aromatic hardener accounts for higher thermal stability compared to an aliphatic one. However, most cured epoxy systems are easily flammable, and thus different flame retardants are used to fulfill stringent requirements in the transport industry [5]. Modern technologies for 5G, next-generation networks, and sensors in packaging for anti-counterfeiting demand for always more multifunctional epoxy coatings able to combine good overall properties with transparency and special functions [6,7]. The addition of flame retardants and other additives into an epoxy matrix allows for the preparation of high-performing flame retardant composite epoxy coatings, though these latter may negatively interfere with the normal packing of polymer chains, often resulting in a detrimental effect on the mechanical behavior [8]. Also, end-of-life multifunctional epoxy coatings cannot be easily reprocessed, due to their permanent cross-linked network and the presence of many additives (e.g., phosphorus-based compounds), which makes their effective reshaping or recovery full of hurdles [9,10]. To overcome these issues, the development of self-

* Corresponding author.
E-mail address: aurelio.bifulco@unina.it (A. Bifulco).

https://doi.org/10.1016/j.cej.2024.149327
Received 4 December 2023; Received in revised form 10 January 2024; Accepted 1 February 2024

responsive transparent flame retardant multifunctional epoxy coatings showing easy reprocessability would be highly desirable [11]. These materials may foster the preparation of safer and more sustainable thermosets, keeping interesting optical characteristics and high overall performances.

Carbon-based nanomaterials, such as graphene, nanotubes, and quantum dots, are gaining increasing interest as functional fillers for conferring specific properties to epoxy resins. Among them, carbon-based sub-ten-nanometer nanoparticles, i.e., the carbon dots (CDs), are emerging as very promising to replace conventional inorganic semiconductor quantum dots. CDs can be obtained starting from different precursors, like small compounds, bio-derived materials, and synthetic polymers. They exhibit outstanding photoluminescence (PL) that has opened their use in sensing and imaging, although this peculiar property depends on the surface functionalization or passivation of the carbon-based nanoparticles and its mechanism has not been clearly explained yet [12]. As the air negatively affects the PL features of CDs, some applications have been recently proposed, in which CDs are incorporated into epoxy matrices [12,13]. Salehtabar and Ghaemy synthesized photoluminescent water-soluble nitrogen-doped CDs derived from gum tragacanth polysaccharide and triethylenetetramine by a one-step hydrothermal carbonization route; the so-obtained CDs were mixed with DGEBA to fabricate transparent composite coatings with high emission quantum yield (74.69 %) at 460 nm [14]. Also, Lee et al. proposed the use of CDs from amine-containing precursors as curing agents of epoxy monomers [15]. The so-prepared CDs could be uniformly dispersed in the epoxy matrix to provide composites with PL intensity retentions beyond 80 % after 8 weeks of storage in ambient conditions, hence showing significant potential for anti-forgery applications [15].

Due to the huge production of epoxy-based items and their complex recycling, the amount of waste has enormously risen over the years. Lowering the flammability of epoxy composites and conferring them the possibility to be reshaped may significantly extend their lifetime. In particular, shape memory polymers (SMPs) are materials able to alter their shape in response to a specific stimulus, therefore they can keep a temporary shape for a long time and recover their permanent shape [16]. Heat stimulus is the most employed, though magnetic fields, light, and pH have also been extensively investigated. A recent study estimates that the shape memory polymer market, which is currently valued at 392.4 million USD [17], is predicted to show a compound annual growth rate of 21.5 % from 2021 to 2027, due to the growing demand for high-performing and commercial shape-morphing products [18]. Due to their properties, SMPs can meet the requirements to be used in biomedical devices, actuators, and textile materials [19,20]. Besides, SMP composites are usually characterized by low production costs, easy processing, and low density. Yadav et al. incorporated carbon fibers (CFs) into an epoxy resin to improve the mechanical properties and shape memory effect [21]. They found out that the addition of 1.5 wt% of CFs could reduce the recovery time up to ~ 42 % [21]. Liu et al. prepared a series of DGEBA-based shape memory nanocomposites cured with methylhexahydrophthalic anhydride [19]. The addition of multi-wall carbon nanotubes (MWCNT at 0.75 wt% loading) into the polymer matrix could significantly increase the mechanical properties at temperatures close to the glass transition, the repetition stability, and the recovery rate of the shape memory cycles [19].

Recently, Guadagno et al. embedded pre-functionalized MWCNT (0.5 wt% loading) in a rubber-toughened epoxy formulation to design self-healing nanocomposites [22]. They demonstrated that suitable fillers can be decorated by covalently bonded moieties able to act as hydrogen bond acceptors and donors [22]. The dynamic reversibility of hydrogen bonds triggered by an external stimulus (e.g., heat) enables the synthesis of shape memory and self-healing materials, where the repetition of the repair events makes possible the reshaping of the final products [23–25]. As their surface chemistry depends on the used raw materials and synthesis route, CDs may be obtained not only at nanometric size but also full of hydroxyls able to establish reversible bonds with both OH groups of cured epoxy and other polar species located in the polymer network [26]. Feng et al. provided shape memory capability to a self-extinguishing epoxy composite, keeping unvaried transparency, glass transition temperature, and mechanical behavior [27]. In particular, DGEBA resin was cured with a 9,10-dihydro-9-oxa-10-phosphaphenanthrene-10-oxide (DOPO)-modified maleic anhydride curing agent, using zinc acetylacetonate hydrate as a catalyst. The application of a high-temperature flame could trigger the shape memory effect of the flame retardant epoxy thermoset, making easy its reshaping, hence demonstrating the suitability of the epoxy system for the manufacturing of fire safety tools [27].

Lately, Passaro et al. obtained hydrophobic epoxy composite coatings by the addition of functionalized hemp microparticles into the matrix. The condensation of hexadecyltrimethoxysilane (HDTMS) with the hybrid hemp microparticles induced their segregation on the surface of epoxy, thus conferring low wettability and anti-icing properties to the final products [28]. Similarly, CDs may be functionalized with a hydrophobic silane and used as a functional additive for DGEBA resin, without any chemical modification, to reduce the wettability, and make more refractory as well as fire resistant the surface of epoxy coatings. Besides, the presence of the CDs embedded into the polymer network may enable the reshaping of the epoxy composite and provide a PL response. This strategy would expand the range of possible applications related to the fabrication of multifunctional epoxy thermosets containing CDs in the sensing and flame retardancy fields.

In this research work, also following a waste-to-wealth approach, we synthesized carbon dots starting from humic acids as bio-waste raw material by a simple one-step hydrothermal route. CDs were further functionalized using HDTMS as a hydrophobic agent and dispersed at two different loadings (namely 0.1 and 0.3 wt%) into a DGEBA resin cured by isophorone diamine (IDA) to obtain epoxy nanocomposites. Both nanocomposites showed PL capability, though only the one with the lowest filler loading showed full transparency. Further, the presence of the CDs in the matrix provided the resulting nanocomposites with flame-triggered shape memory effect, together with hydrophobicity and fire-resistant properties. This multifunctional epoxy thermoset was applied as a protective coating on polypropylene films used for packaging to demonstrate its suitability for sensing, flame retardant and anti-counterfeiting applications. Structural features, morphology, and chemical composition of CDs, epoxy nanocomposites, and residual chars were investigated by spectrophotometric and microscopy techniques. The thermal behavior, switch temperature, and shape recovery rate of epoxy nanocomposites before and after flame recovery were thoroughly studied. A gas torch coupled with an IR-camera was employed for assessing the fire resistance of the composite surface by measuring the back temperature and its profile along the time. Cone calorimetry tests were carried out to shed light on the fire behavior of the obtained nanocomposites. Finally, the mechanical behavior of epoxy nanocomposites before and after flame recovery was assessed through flexural tests. All these research outcomes clearly highlighted the “all-in-one” multifunctionality provided by the designed nanocomposites that may pave the way toward advanced applications.

2. Materials and methods

2.1. Materials

A two-component epoxy resin system (SX10) made of a modified diglycidyl ether of bisphenol-A (DGEBA) resin and isophorone diamine (IDA), a cycloaliphatic diamine hardener, purchased from MATES S.r.l. (Milan, Italy), was employed. Hexadecyltrimethoxysilane (HDTMS) (>85 %), humic acid sodium salt (HASS), and acetone were purchased from Sigma-Aldrich (Merck KGaA, Darmstadt, Germany) without further purification.

2.2. Synthesis of carbon dots

Carbon dots (CDs) were synthesized through a hydrothermal route starting from HASS as an organic precursor. For this purpose, 0.125 g of HASS were dispersed in 62.5 mL of bidistilled H_2O under stirring for 10 min. Then, the suspension was transferred into a 75 mL Teflon-lined stainless-steel autoclave and heated at 200 °C for 24 h. Next, the autoclave was allowed to naturally cool to room temperature and the obtained brown solution was centrifuged at 10000 rpm for 15 min to separate large particles, while the supernatant was recuperated and further subjected to a double-step process based on tip-sonication for 15 min and filtration through filters with pores of 0.45 μm to break the clusters and remove the largest particles.

2.3. Preparation of epoxy nanocomposites and coatings containing carbon dots

Fig. 1 displays the main steps of the procedure for preparing epoxy nanocomposites containing carbon dots. As reported in Table 1, the blank epoxy sample (E) was obtained by mixing a specific amount of DGEBA resin with acetone, deionized water, and IDA (26 wt% of the epoxy). The mixture was poured into a silicone rubber mold (5 × 5 × 0.3 cm^3), then cured overnight (~12 h) at 28 °C. Carbon dots were used as a filler for the synthesis of DGEBA-based epoxy nanocomposites, at two different loadings, namely 0.1 wt% (ECD0.1) and 0.3 wt% (ECD0.3). A typical formulation was prepared via a one-pot method by incorporating 0.1 or 0.3 wt% of CDs, 5 wt% of acetone, 1.5 wt% of water, and 1.0 wt% of HDTMS into a certain amount of DGBEA resin (Fig. 1 and Table 1). Similar to ECD0.1 and ECD0.3, an epoxy sample filled with acetone, water, and HDTMS (ESil) and one containing acetone, water, and 0.3 wt % CDs (E-CD) were prepared as counterparts to elucidate the effect of these additives on the overall properties of the final cured systems. The addition of water and acetone was found to be crucial to obtain a uniform distribution of CDs within the epoxy matrix, but also to lower the viscosity of the resin system. The curing conditions of ECD0.1 and ECD0.3 were the same used for the blank epoxy sample.

Table 1
Nominal chemical compositions of the prepared epoxy nanocomposites.

Sample	DGEBA (g)	IDA (g)	CDs (wt.%)	Acetone (wt.%)	Water (wt.%)	HDTMS (wt.%)
E-NC	7.5	–	–	–	–	–
E	7.5	1.95	–	5	1.5	–
ESil	7.5	1.95	–	5	1.5	1.0
E-CD	7.5	1.95	0.3	5	1.5	–
ECD0.1	7.5	1.95	0.1	5	1.5	1.0
ECD0.3	7.5	1.95	0.3	5	1.5	1.0

Weight percentages are calculated on (DGEBA + IDA) base. E-NC refers to the uncured epoxy resin.

2.4. Shape recovery and fire resistance evaluation

To investigate the heat/flame-shape recovery effect of ECD0.1 and ECD0.3, both samples (5 × 1 × 0.3 cm^3 size) were heated to 100 °C (i.e., over the glass transition temperature of the material, see section 3.3) in a well-controlled heating chamber and programmed from the original/permanent flat shape (Fig. 1), assumed during the curing process, to a temporary bent shape. The programming process was performed by pressing the sample against a small steel cylinder (with an angle of ~ 75°) during the cooling of the nanocomposite down to room temperature (~27 °C). The temperature of the samples was measured by an infrared thermometer during each step of the shape programming procedure. The samples that underwent flame-triggered shape recovery one time were coded ECD0.1-1R and ECD0.3-1R, while the ones subjected to three recovery cycles were named as ECD0.1-3R and ECD0.3-3R.

Finally, to perform wettability, fire resistance, and shape recovery tests, some polypropylene (PP) films (300 × 20 × 0.2 mm^3) were used as packaging substrates and coated with the one-pot formulations: this way it was possible to study the hydrophobicity and the fire response of E and ECD0.1 employed as protective and anti-counterfeiting coatings. Before starting the deposition, the formulations were stirred and sonicated to obtain degassed homogeneous systems. Then, thin layers of ECD0.1 and E (used as a reference) were deposited on specific sections of the PP

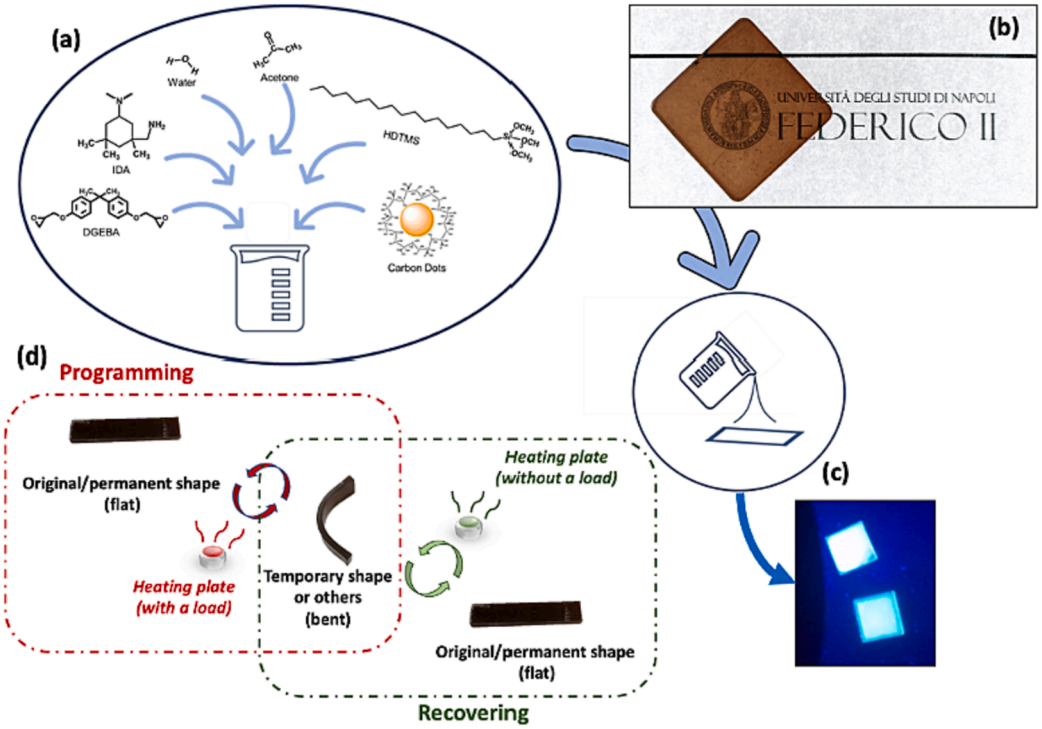

Fig. 1. One-pot fabrication of epoxy nanocomposites containing carbon dots (a), exhibiting: high transparency (b), photoluminescence under UV irradiation (c), and shape recovery features (d).

substrate and cured following the same procedure adopted for the bulk samples.

2.5. Physicochemical characterization of materials

2.5.1. Analysis of CDs

Transmission electron microscopy (TEM) was carried out to assess the morphology and size of CDs. A small amount of the obtained suspension was deposited onto copper meshes and examined in bright field mode with a FEI TecnaiG12 Spirit Twin TEM running at 120 kV acceleration voltage.

X-ray diffraction (XRD) was performed to investigate the crystalline structure of CDs by using a Malvern PanAnalytical diffractometer (Malvern, UK) with a nickel filter and Cu K-α radiation.

Fourier-transform infrared (FTIR) spectra of CDs as powdered samples were obtained using a Nicolet 5700 FT spectrometer (ThermoFisher, Waltham, MA), to confirm the formation of carbonaceous nanomaterials as well as to identify the surface functional groups.

UV-Visible (UV–Vis) spectra of CDs were acquired in the 190–800 nm range using a SHIMADZU UV-2600i spectrophotometer (Shimadzu, Milan, Italy). In particular, 1.0 mL of suspension of CDs was placed in a quartz cuvette to carry out the measurements.

The **fluorescence** spectra of CDs were recorded at 25 °C using a Horiba Scientific Fluoromax-4 spectrofluorometer equipped with a Peltier control system and 1 cm path length cells. The CDs suspension was excited to the specific absorption wavelength, determined by means of UV–Vis spectroscopy measurements (integration time: 0.1 s, excitation and emission slit width: 5 nm).

2.5.2. Characterization of the epoxy-based nanocomposites

FTIR spectra in Attenuated Total Reflectance (ATR) mode of all the prepared samples were obtained using a Nicolet 5700 FT spectrometer (Thermo Fisher, Waltham, MA) to confirm the completeness of the curing procedure and the chemical composition as well. All of the spectra were collected using the Thermo Scientific OMNIC Software Suite with 32 scans and a resolution of 4 cm^{-1}. The C = C bonds of the benzene rings found in the epoxy resin structure, which are not affected by the curing reactions, were associated with some specific bands in the spectrum, namely 1607 and 1509 cm^{-1}, and used to normalize the spectra. Also, the chemical features of residual chars produced by cone calorimeter tests were analyzed by FTIR spectroscopy.

UV–Vis transmittance spectra of the nanocomposites were collected on thin samples (size: 20 × 20 × 0.7 mm^3) in the 200–800 nm range by means of a SHIMADZU UV-2600i spectrophotometer (Shimadzu, Milan, Italy) equipped with an ISR-2600Plus two-detector integrating sphere.

To determine the **wettability** of pure resin and epoxy nanocomposites, a Dataphysics OCA 30 instrument was used. The water contact angle (WCA) was measured at around 21 °C and evaluated by posing liquid droplets with a volume ranging from 6 to 9 μL on the surface of thermosetting substrates [29].

Dynamic mechanical analysis (DMA) was carried out on rectangular specimens (size: 35 × 10 × 4 mm^3) using a Q800 TA Instrument (New Castle, DE, USA) in the single cantilever mode to evaluate the storage (E′) and loss moduli vs. temperature of pristine resin and epoxy nanocomposites. All the thermosetting samples were characterized using a ramp-up of temperature from 30 to 150 °C at 2 °C/min and 1 Hz of frequency. The temperature, at which the highest damping occurs (i.e., tan δ max), was employed for evaluating the glass transition temperature (Tg) of the prepared epoxy systems.

Thermogravimetric analysis (TGA) was carried out to study the pyrolytic degradation behavior of the unfilled cured resin and its nanocomposites. For a typical measurement, 10 mg of sample was analyzed in a TA Instrument simultaneous thermoanalyser SDT Q600 under N_2 with a flow of 50 mL/min, and in the temperature range from 25 to 800 °C with a heating rate of 10 °C/min.

The surface chemistry and the residual char morphology of both unfilled resin and its nanocomposites were examined using an EVO 15 **scanning electron microscope (SEM)** from Zeiss (Oberkochen, Germany). An Ultim Max 40 **energy-dispersive X-ray (EDX)** microanalyzer was coupled with the microscope, integrated with AZtecLive software released by Oxford Instruments (High Wycombe, UK).

A **cone calorimeter** (Noselab ATS, Monza, Italy) operating with an irradiative heat flux of 35 kW/m^2 (ISO 5660 standard) was exploited to evaluate the fire behavior of pristine resin and epoxy nanocomposites. The specimens (10 × 10 × 0.3 cm^3) were laid horizontally using a grid. The cone calorimetry tests were performed to determine the time to flame out (TTFO, s), time to ignition (TTI, s), total heat release (THR, MJ/m^2), heat release rate (HRR, kW/m^2), peak of the heat release rate (pkHRR, kW/m^2), total smoke release (TSR, m^2/m^2), carbon monoxide yield (CO yield, kg/kg), carbon dioxide yield (CO_2 yield, kg/kg) and specific extinction area (SEA, m^2/kg).

Burn-through tests were performed on pristine resin and epoxy nanocomposites to assess their burn-through resistance toward the application of a flame to the front side. The test was carried out using a small-scale butane burner apparatus (Cadrim, China). The burner system generated a flame with a temperature about 1200 °C and a front heat flux of 170 kW/m^2. The rear or back-side temperatures of two sets of three specimens (10 × 10 × 0.3 cm^3) and their corresponding ignition and burn-through times were monitored by a digital data acquisition system and an **InfraRed camera** also working as thermometer (NEC Avio Infrared Technologies CO., Ltd., Thermo Gear G100/G120, Tokyo, Japan). The burn-through test was conducted according to the configuration shown in scheme S1. The fire resistance in terms of **surface flammability** of virgin resin and thermosetting nanocomposites was evaluated by applying the flame tip of a butane gas lighter in the middle of their surface. The time until the sample captured the flame and started burning was recorded. The test was performed on two sets of three specimens (5 × 1 × 0.3 cm^3) for each sample.

Three-point bending tests were performed according to ISO 178 standard by using an MTS Insight 30 testing machine [30]. All the experiments were conducted at room temperature (22 °C) and under displacement control by imposing the speed of 1 mm/min. The specimens' nominal thickness h, width b, and length l were equal to 3, 10, and 60 mm, respectively. A support span L of 45 mm was used. Bar-shaped samples were made using a silicone mold and cured at controlled temperature and humidity. The flexural stress and strain were calculated using the following formulas:

$$\sigma_f = \frac{3FL}{2bh^2} \tag{1}$$

$$\epsilon_f = \frac{6\delta h}{2b} \tag{2}$$

where F is the applied force and δ is the deflection of the beam, i.e., the crosshead displacement. The Modulus of elasticity resulted from the equation:

$$E_f = \frac{\Delta\sigma_f}{\Delta\epsilon_f} \tag{3}$$

where the differences in flexural stress $\Delta\sigma_f$ were evaluated in correspondence with given flexural strains. A different method for the calculation of flexural modulus, based on the classical beam theory approach, is provided by the ASTM D790 standard [31]:

$$E_f = \frac{mL^3}{4bh^3} \tag{4}$$

where m is the slope of the tangent to the initial straight-line portion of the load–deflection curve. Negligible differences were found in the results of the experimental activity between the flexural modulus values assessed by the two methods.

3. Results and discussion

3.1. Morphological, surface, and optical properties of CDs

The morphology and dimension of the obtained CDs were characterized by TEM, as reported in Fig. 2a. The formation of monodisperse pseudo-spherical nanoparticles was observed, with an average size of about (10 ± 2) nm. The crystalline nature of CDs was further characterized by XRD analysis. As shown in Fig. 2b, a broad peak centered at 2θ = 25.81° was observed in the pattern: it corresponds to an interlayer spacing of 0.36 nm and can be assigned to graphite (002) planes, in agreement with previous results obtained for CDs synthesized under different conditions [32,33]. The peaks are broad due to the small size of CDs and the high value of the interlayer distance, probably ascribed to the presence of oxygen functional groups. Indeed, the FTIR spectrum (Fig. 2c) shows the peak at about 3408 cm^{-1}, which is related to the stretching of O–H bonds, while the peak at about 1384 cm^{-1} is ascribable to vibrations of –COOH groups. Both these peaks indicate the presence of carboxylic and hydroxyl groups on the particles' surface [34], supporting the evidence of an easy water-dispersibility of hydrothermally synthesized CDs. The emerging peaks at about 2980 and 2854 cm^{-1} are associated with stretching vibrations of C–H bonds, and the peak due to C = C bond vibrations of benzene rings appears at 1600 cm^{-1}. The peaks at about 1026 cm^{-1} are assigned to the C–O stretching vibrations belonging to primary-OH groups [34].

As far as the optical properties are considered, Fig. 2d shows the UV–Vis absorption spectrum of CDs in an aqueous solution. The single peak centered at about 260 nm is due to a π-π* transition of aromatic C = C bonds and agrees with previous evidences [34,35]. By exciting at the absorption wavelength, the CDs suspension shows an emission peak centered at about 451 nm (Fig. 2d), which is mainly due to the presence of aromatic conjugated structure, quantum size effect, oxygen-containing groups and, possibly, surface defects acting as emission traps [34,35].

3.2. Surface analysis and wettability of epoxy nanocomposites containing CDs

The epoxy-based nanocomposites appear as homogeneous and transparent panels (see Fig. 1b), although the sample with the highest content of carbon dots (i.e., ECD0.3) shows a more evident brown coloration that suggests the formation of some small aggregates of CDs dispersed in the matrix. The optical properties of pristine resin (E) and epoxy nanocomposites (ECD0.1 and ECD0.3) were investigated by UV–Vis spectroscopy. Transmittance spectra (Fig. S1) of thin samples confirm the high transparency in the visible range of ECD0.1, whose average transmittance between 400 and 800 nm is 79 %, close to that of E (86 %). On the other hand, the higher amount of CDs in ECD0.3 and the consequent formation of aggregates lead to scattering phenomena, resulting in a decrease in the average transmittance (to about 62 %). Besides, in agreement with the fluorescence features of CDs (section 3.1), the addition of the prepared carbonaceous small nanoparticles, acting as fluorescent fillers, allows to obtain photoluminescent nanocomposites yielding a blue emission under UV illumination (see Fig. 1c).

The chemical structure of the materials was analyzed by ATR-FTIR spectroscopy. Fig. S2 shows the spectra of ECD0.1 and ECD0.3, together with those of the blank epoxy resin (E) and uncured DGEBA (E-NC). The effective cross-linking of the epoxy through the cure with the cycloaliphatic amine hardener is witnessed by the disappearance of the band at 912 cm^{-1}, corresponding to the stretching of the oxirane ring, and by the broad band arising around 3400 cm^{-1}, due to the hydroxyl groups formed during the ring-opening reaction. No visible differences are seen between the spectra of the cured samples, indicating that the presence of the fillers does not alter the chemical profile of the resin,

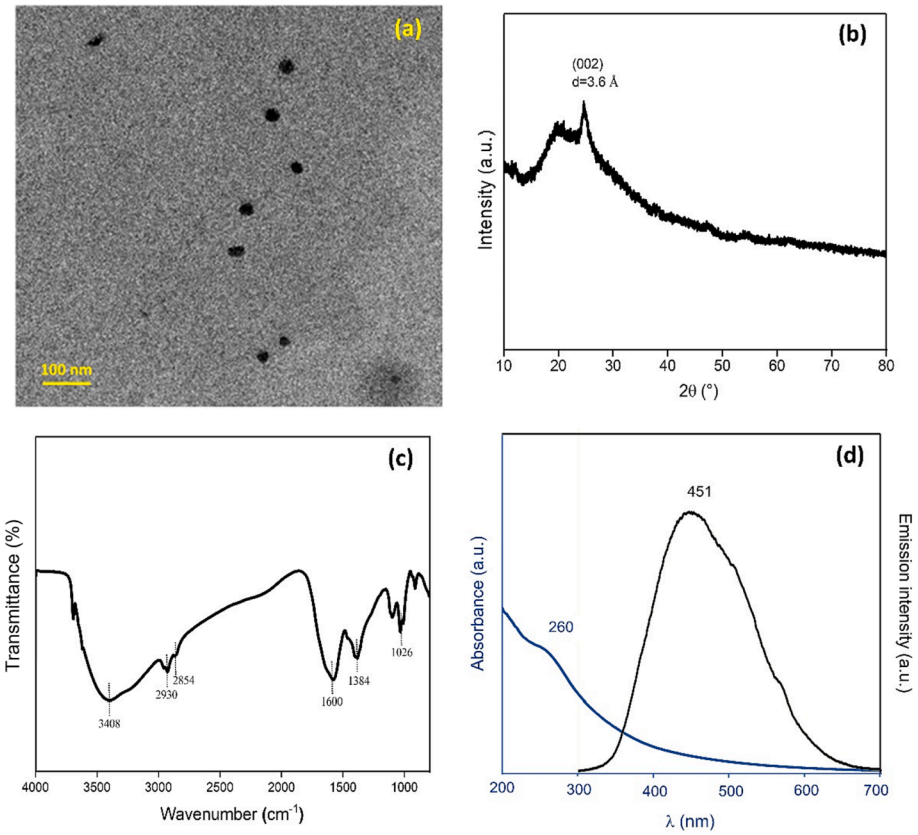

Fig. 2. TEM morphology of CDs (a), crystalline structure by XRD (b), surface chemistry by FTIR (c), and absorption/emission behavior by UV–Vis and fluorescence spectroscopy (d).

while their concentrations are too low to produce detectable vibrational bands. The achievement of a complete cure of the nanocomposites despite the low curing temperature (28 °C) is further confirmed by DSC curves (Fig. S3), which highlight the absence of any residual exothermic peaks associated with further cross-linking in the first heating ramp.

The surface morphology and composition of the epoxy nanocomposites were investigated by SEM-EDX analysis. Fig. 3 reports the SEM images and elemental distribution of the surface for ESil, ECD0.1, and ECD0.3. ESil presents a rather smooth surface, which seems to become rougher with increasing the CD content. It is interesting to note the surface concentration of silicon in the three samples. As it derives from the silane only, EDX results seem to indicate the presence of HDTMS not only on the outermost layers of the samples but also in their bulk. The estimated concentration of Si in ESil (0.1 wt%) is, indeed, close to the nominal value, suggesting a uniform dispersion of HDTMS in the bulk of the material. The higher contents of Si detected for ECD0.1 and ECD0.3 reveal the crucial role of CDs in modifying the distribution of HDTMS [28,36,37]. As a matter of fact, the higher the loading of CDs into the epoxy matrix, the larger the amount of HDTMS located in the surface layer, with a good uniformity evidenced by the EDX maps shown in Fig. 3. This correlation provides evidence for the interaction between the nanoparticles and the silane molecules. A certain amount of HDTMS is likely hydrolyzed by the water added to the system and its silanol groups can condense with hydroxyls of CDs during the curing process. Hence, a functionalization of CDs occurs *in situ* through the formation of chemical or physical bonds (i.e., hydrogen bonds). This association can foster the migration of the filler, partly covered by the alkyl chains of HDTMS, to the surface of the epoxy resin.

The wettability of the composite surface is expected to be affected by the exposure of CDs and silane. This property is commonly evaluated by means of the water contact angle (WCA), which represents the angle formed between the outline of the contact surface and the surface of the liquid. On the basis of the WCA value, a surface can be categorized as hydrophilic ($\theta < 90°$) or hydrophobic ($\theta > 90°$), while extremely hydrophobic surfaces provide a WCA $\geq 150°$. Fig. 3 displays the results of static water contact angle measurements performed on the epoxy nanocomposites (ECD0.1 and ECD0.3), and, for comparison, on E, ESil, and an epoxy sample filled by 0.3 wt% of CDs alone (E-CD). For epoxy samples containing the same amount of HDTMS in their formulations (namely, ESil, ECD0.1, and ECD0.3), the addition of CDs up to 0.3 wt% led to a striking progressive increase of WCA, where ECD0.3 exhibited a contact angle close to 150°, revealing an almost superhydrophobic surface. Also, Fig. 3 shows that the incorporation of CDs alone could not lower the wettability and thus increased the WCA of the epoxy resin. As previously mentioned in section 3.1, the surface of CDs is fully decorated by hydroxyl groups, conferring polar characteristics to the nanostructures. These chemical features of CDs are responsible for their migration at the interface with air. For this reason, the epoxy sample containing CDs alone exhibited a WCA lower than that of the unfilled resin, whose surface still shows a typical prevalently non-polar nature. Based on the Cassie–Baxter model, a non-textured surface can only lead to a maximum WCA of around 130°, whereas higher WCAs require both a rough surface and the support of an efficient hydrophobizing and water repellent additive (e.g., fluorine-based or alkyl silanes) [38–40]. Therefore, the higher WCA of ECD0.3 than ECD0.1 might be ascribed to the greater content of CDs, giving rise to a rougher surface texture on the former nanocomposite (see SEM images in Fig. 3). On the other hand, the concentration of the nanoparticles at the surface brings an increasing amount of bound HDTMS to be exposed, in agreement with EDX results.

This phenomenon in combination with a rougher surface may represent the chemical and morphological contributions responsible for the higher hydrophobicity of ECD0.1 and ECD0.3, with respect to pristine resin and other thermosets (ESil and E-CD) [41,42]. As a high hydrophobicity was one of the main objectives of this study, the E-CD sample exhibiting hydrophilic character was not further investigated.

3.3. Thermal behavior of epoxy nanocomposites containing CDs

Dynamic mechanical analysis was performed to evaluate the viscoelastic response of E, ECD0.1, and ECD0.3 as a function of temperature. The maximum of tan δ curves and the corresponding temperatures were determined to evaluate the glass transition temperature values (Fig. 4a). With respect to ECD0.1 and ECD0.3, E exhibits the highest tan δ values (tan δ peak centered at 75 °C) and is characterized by a narrow and

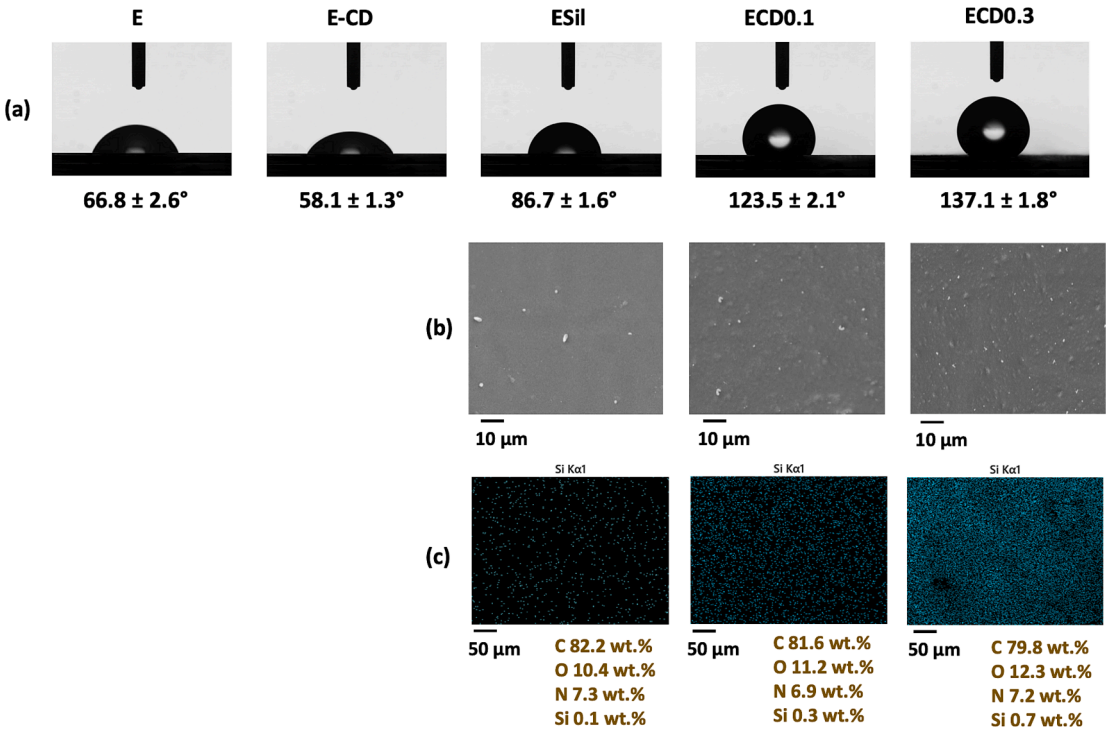

Fig. 3. Pristine resin, epoxy resin filled by HDTMS, and epoxy nanocomposites containing carbon dots: water contact angles (a), SEM images (b) and EDX maps (c).

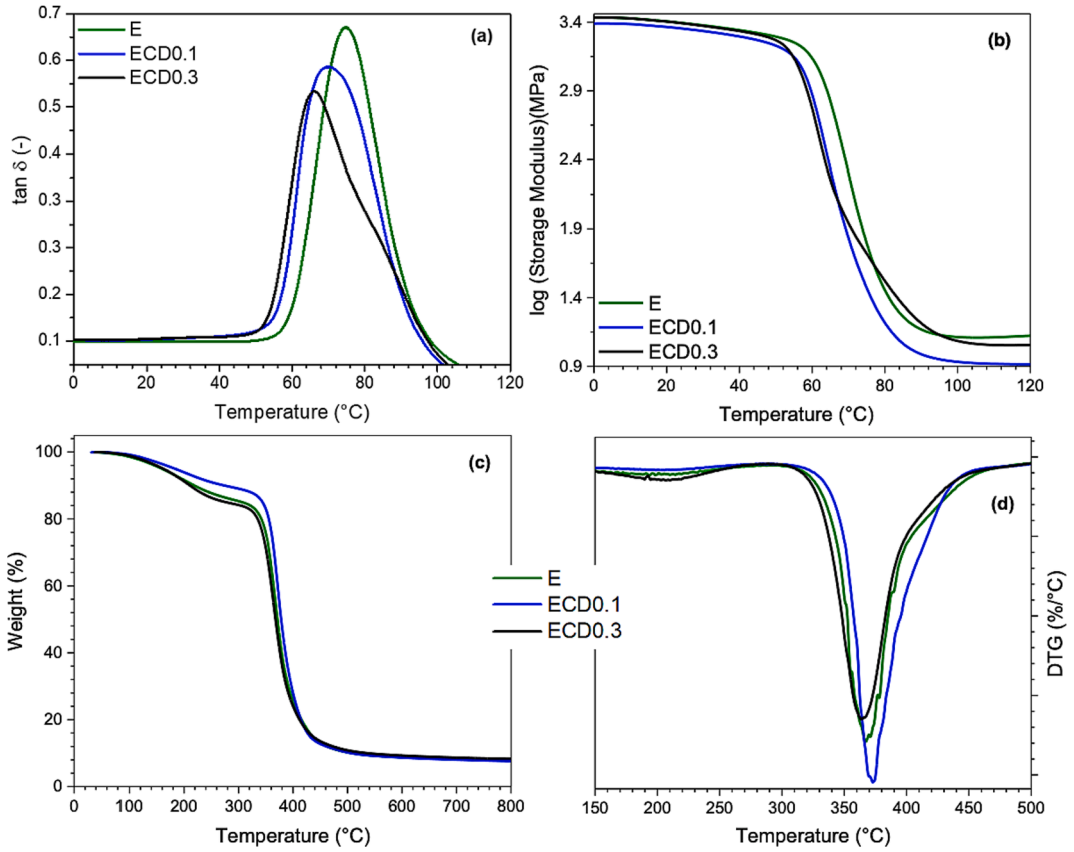

Fig. 4. Tan δ vs. temperature curves of pristine resin and epoxy nanocomposites (a), storage moduli (E′) vs. temperature of pristine resin and its nanocomposites (b). TGA (c) and DTG (d) curves in nitrogen.

symmetric curve, revealing that such material can easily dissipate the application of a load by segmental motions (i.e., energy dissipation mechanisms) [43]. Conversely, the tan δ curves of epoxy nanocomposites seem to be affected by a broad distribution of relaxation phenomena, especially the one referred to ECD0.3, probably due to the presence of CDs limiting the molecular motion of polymer chains and providing more elastic features to both materials [44–46]. The presence of the CDs in the epoxy matrix disturbs the inter-chain interactions and thus the packing of chains in the polymer matrix, reducing the ability of ECD0.1 and ECD0.3 to dissipate the energy received from a load application [47]. This effect of CDs on the polymer network results in slightly lower glass transition temperatures of ECD0.1 and ECD0.3 (respectively, 70 °C and 66 °C), compared to unfilled epoxy resin (Fig. 4a).

The tan δ curve of ECD0.3 shows the presence of a shoulder at higher temperatures, which may be seen as a second glass transition temperature ($Tg_{(ECD0.3)2} = 86$ °C). CDs dispersed throughout the polymer matrix are able to establish hydrogen bonds with the hydroxyl groups formed during the cross-linking process [1,48]. Despite the very low CD loadings (not exceeding 0.3 wt%), these physical interactions significantly stiffen the epoxy system. This stiffening effect was also found in other epoxy systems containing hybrid organic–inorganic phases or well-embedded nanostructures [46,49,50]. Conversely, the very low amount of CDs in ECD0.1 does not cause the appearance of a second Tg, though the presence of hydrogen bond interactions in such a system cannot be excluded [1].

These findings well agree with the storage moduli (E′) collected as a function of temperature in Fig. 4b. ECD0.1 shows the lowest values of E′ in the glassy state region, likely due to the low loading of CDs, leading to a predominant disturbance effect of inter-chain interactions in the polymer network compared to the stiffening effect. This latter becomes predominant in the case of ECD0.3, where the higher amount of CDs enables the establishment of more hydrogen bonds, resulting in E′ values quite similar to those of unfilled resin (Fig. 4b). However, a limited content (0.1, 0.3 wt%) of CDs does not significantly affect the storage modulus profile of epoxy: therefore, based on the DMA results, it may be argued that the incorporation of very low amounts of CDs into the polymer matrix marginally worsens the mechanical properties of the resulting materials. This is also confirmed by the flexural stress at 5 % strain of E, which is only 17 % and 29 % higher than those of ECD0.1 and ECD0.3, respectively (Table 3 in section 3.5). Besides, ECD0.1 and ECD0.3 were found to have a slightly lower bending modulus of 8 % and 16 %, respectively, in comparison to that of the pristine resin.

Fig. 4c shows the results of the thermogravimetric analyses performed on both unfilled epoxy and its nanocomposites containing CDs. The measurements were conducted under N_2 atmosphere to highlight the effects rising from the addition of carbon dots on the pyrolytic decomposition of epoxy. Also, Fig. 4d reports the derivative thermogravimetric (DTG) curves of E, ECD0.1 and ECD0.3. The incorporation of CDs into the epoxy matrix results in a remarkable increase in the initial decomposition temperature compared to the pristine resin, especially with 0.3 wt% filler content ($T_{5\%}$ +14 %, $T_{10\%}$ +25 %, see Table 2). CDs strongly affect the pyrolytic decomposition of the polymer matrix, delaying the start of the devolatilization phenomena, probably due to their capability to slow down the heat exchange at the boundary layer. This thermal shielding effect of CDs, mainly exerted by those located at the surface of epoxy nanocomposites, may be linked to their graphitization (see section 3.1) and silane functionalization [15,51,52]. This shielding effect is more effective in the case of ECD0.3, owing to the largest amount of CDs enhancing the thermal stability of the polymer matrix. However, the use of CDs does not lead to a significant increase in the residual char (Table 2), additionally supporting that the filler mainly

Table 2
TGA analysis of all samples in N_2. $T_{5\%}$ is the temperature, at which 5 wt% loss is recorded.

Sample	$T_{5\%}$ (°C)	$T_{10\%}$ (°C)	T_{max} (°C)	Residue (wt.%) at	
				T_{max}	800 °C
E	160	218	365	52	8
ECD0.1	165	210	369	54	8
ECD0.3	183	273	372	59	9
ECD0.1-3R	195	293	370	62	9
ECD0.3-3R	198	298	372	64	12

T_{max} is the temperature, at which the weight loss rate reaches the maximum; the residues at T_{max} and 800 °C are also reported.

Table 3
Flexural properties of E, ECD0.1 and ECD0.3 samples.

Sample	σ_f (MPa)	95 % C.I. (MPa)	E_f (GPa)	95 % C.I. (GPa)
E	62 ± 1	1	1.62 ± 0.12	0.14
ECD0.1	51 ± 3	3	1.50 ± 0.06	0.06
ECD0.1-1R	37 ± 2	3	1.03 ± 0.04	0.04
ECD0.1-3R	47 ± 5	5	1.40 ± 0.11	0.12
ECD0.3	44 ± 5	5	1.37 ± 0.12	0.13
ECD0.3-1R	44 ± 3	3	1.13 ± 0.12	0.12
ECD0.3-3R	45 ± 3	3	1.21 ± 0.16	0.18

influences the surface properties of the nanocomposites.

3.4. Switch temperature and heat-triggered shape recovery effect

Based on their chemical structure, shape memory polymers can be classified as thermosetting or thermoplastic SMPs. The switch temperature (T_{sw}) is the temperature, at which the sample starts recovering its original shape, moving from a temporary geometry. The T_{sw} of thermoset SMPs is usually the glass transition temperature, whereas in the case of thermoplastic SMPs can be either the crystal melting temperature or the Tg [19,53]. Thermoplastic SMPs are mostly used in civilian commodities, while thermoset shape memory epoxies are largely employed in the aerospace industry, as these materials are generally characterized by easy manufacturing and high T_{sw}, shape recovery rate, and dimensional stability [54]. To assess the T_{sw} and the shape recovery rate of ECD0.1 and ECD0.3, several experimental trials were performed. Before starting the experiments, ECD0.1 and ECD0.3 were programmed to a temporary bent shape (Fig. 5, where $Tg_{ECD0.1}$, $Tg_{ECD0.3}$, and Tg_E represent the glass transition temperatures of ECD.01, ECD0.3 and E measured by DMA), according to the procedure reported in section 2.4. The heating of pristine epoxy and ESil made the samples very rigid and brittle, therefore they could not be programmed (Fig. 1) and reshaped. Bent ECD0.1 and ECD0.3 were dipped into a water bath kept at different temperatures and the time required to recover the original flat shape was collected (see Video 1). These measurements were repeated three times to assess their reproducibility and accuracy. Fig. 5 reports the variation along the temperature of this shape recovery time (SRT). When the bath temperature was kept close to the Tg values of epoxy nanocomposites, the SRT strongly reduced, and an almost immediate shape recovery was observed. Thus, in agreement with other results in the literature [19,53], T_{sw} values of ECD0.1 and ECD0.3 can be considered basically the same as their glass transition temperatures. The incorporation of CDs, together with HDTMS, acetone, and water, into the epoxy matrix led to very low SRTs at T_{sw}, namely of 15 s and 18 s, for ECD0.1 and ECD0.3, respectively. The rapid response to the heat stimulus (Fig. 5) of the epoxy nanocomposites was obtained without any chemical modification of the polymer matrix, and even with only very low loadings of CDs.

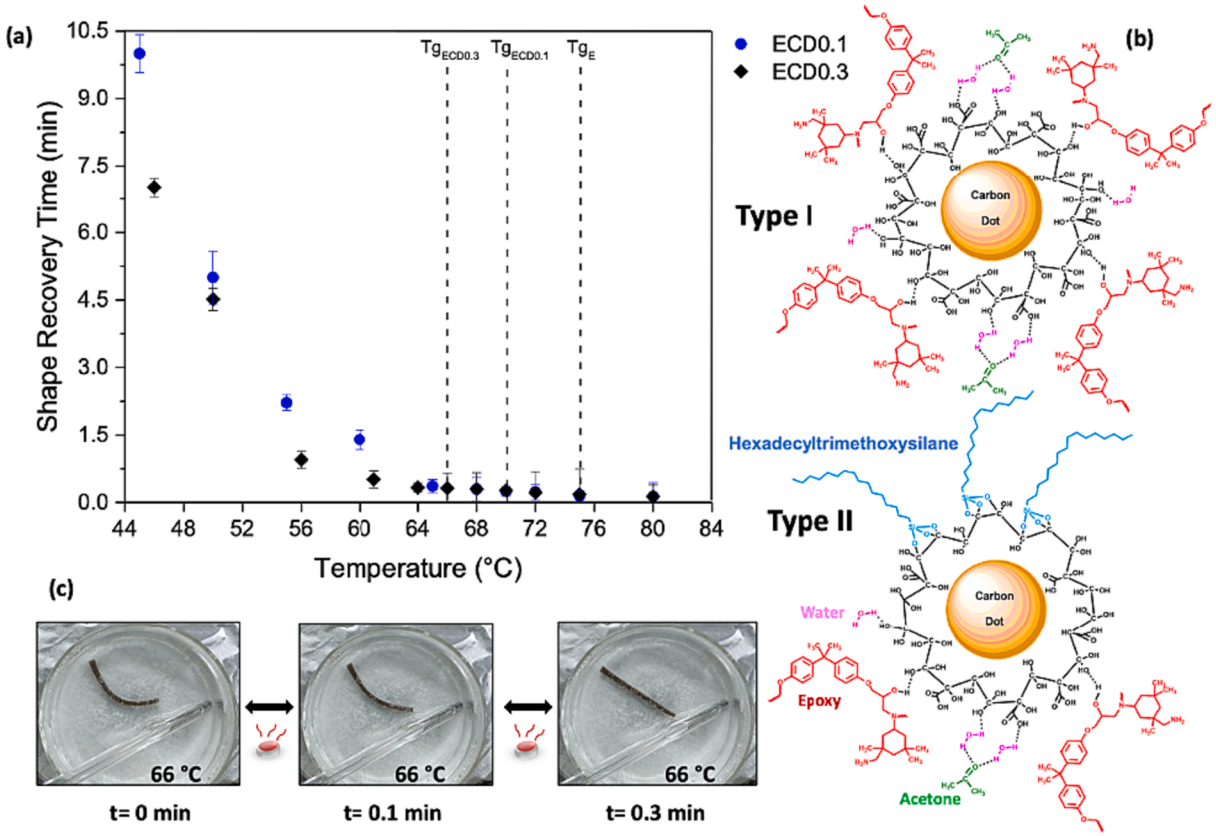

Fig. 5. Experimental trials by heat induction in a water bath for the identification of the switch temperature of the epoxy nanocomposites. Shape recovery time at a specific temperature of the water bath (a), exemplificative representations of possible hydrogen bonding interactions (b). Shape recovery vs. time for ECD0.3 at 66 °C (c).

As previously mentioned, the surface chemistry of the carbon dots strongly depends on the adopted synthesis methodology and raw materials. Water and acetone were used for the preparation of ECD0.1 and ECD0.3 to make the uncured systems more fluid and enhance the dispersion of CDs. Besides, both solvents promote the formation of reversible hydrogen bonding interactions in the cured thermosets. As shown in Fig. 5, acetone and water can establish H-interactions with the hydroxyl groups of the cured resin and the hydroxyls present on the surface of CDs (see section 3.1). These latter can also give rise to hydrogen bonding interactions with the hydroxyl groups belonging to the cross-linked epoxy chains. Moreover, partially hydrolyzed HDTMS moieties bear available silanol (Si-OH) groups that can participate in these interactions, besides binding to the CDs' surface. Therefore, the dynamic network arises from the presence of different hydrogen bond acceptors and donors in the thermosetting formulations. Finally, it may be hypothesized that two types of functionalized CDs will randomly form: one mostly located in the bulk of the polymer matrix, enabling the repetition of the repair events of the physical netpoints in the network, and another still exhibiting free hydroxy groups able to migrate to the composite surface. This latter is also partially decorated by silanizing agents. As the carbon dots show nanometric size, their active surface is significant, which implies that both types of nanostructures deeply modify the properties of the epoxy nanocomposites. It is reported in the literature that char residues showing high graphitization degree are very effective oxygen and thermal barriers [55,56], especially slowing down the heat exchange phenomena during the combustion of polymer systems. In agreement with the results from thermogravimetric analyses, the graphitic character of CDs may enable them to exert a strong flame retardant action in the condensed phase of burning nanocomposites [8], lowering their surface flammability.

The first type of CDs is responsible for the dynamic reversibility and reshaping features of ECD0.1 and ECD0.3, which become even more pronounced in thin nanocomposite layers (see Video 2), whereas the second one confers hydrophobicity and fire resistance to their surface, due to a shell composed of long silicon-containing aliphatic carbon chains, belonging to HDTMS, and a graphitized structure [14,57]. The occurrence of such mechanisms may provide a reasonable explanation for the heat-triggered shape recovery response observed for the epoxy nanocomposites in the water bath. Fig. 5 shows that keeping the bath temperature in a range between 44 and 62 °C, the shape recovery times of ECD0.3 are significantly lower than those of ECD0.1, which may be ascribed to the higher amount of carbon dots embedded in the polymer network, providing superior dynamic reversibility. These differences in terms of SRTs pale into insignificance when the bath temperature approaches the glass transition, as the mobility of the polymer chains remarkably increases, leading to a less viscous system with more homogeneous physico-chemical properties.

3.5. Surface flammability and flame-triggered shape recovery effect

The surface flammability of E, ESil, and the epoxy nanocomposites was assessed by applying the flame tip of a gas lighter in the middle of their surface and measuring the time to flaming combustion (TTFC) for each sample. Fig. S4 reports some typical photos showing the main stages of the flammability test, together with an average time referred to a specific instant. Unlike E and ESil, epoxy nanocomposites (ECD0.1 and ECD0.3) still do not capture the flame after 25 s, due to combined flame retardant actions of silane species and carbon dots. The presence of the silanol groups in the epoxy matrix of ESil confers acidic characteristics to its polymer network, causing the anticipation of the decomposition ESil compared to E [58,59]. This earlier decomposition anticipates the release of flammable gases and thus the occurrence of flaming combustion. The addition of CDs results in a remarkable increase in the TTFC up to ~ 76 %. Functionalized carbon dots show on their surface silane molecules and residual hydroxyl groups, promoting the dehydration of the epoxy matrix during its burning [60,61]. As previously mentioned, they are mainly located at the surface of the epoxy nanocomposites, hence exerting both charring and thermal shielding effects even from the first combustion stages. As these flame retardant mechanisms are due to the tailored filler, the TTFC increases with the content of carbon dots incorporated into the polymer matrix.

The flame-triggered shape recovery (FTSR) behavior could be studied only for ECD0.1 and ECD0.3, as it was not possible to obtain bent specimens for E and ESil. ECD0.1 and ECD0.3 bent-shaped samples were fixed to a holding clamp in a vertical position and the flame tip of a gas lighter was applied by moving it along the surface of the samples, namely from the clamp to the bottom, till the flat shape could be recovered (Fig. 6, Video 3). The high TTFC values of ECD0.1 and ECD0.3 account for the occurrence of the FTSR of both samples without any burning.

Similarly to the results observed in the case of the heat-triggered shape recovery (section 3.4), ECD0.3 exhibits lower SRT values compared to ECD0.1. The highest loading of CDs into the epoxy matrix leads to a faster reshaping, induced by the flame stimulus, and an important decrease in the SRT (by about 29 %). The results of FTSR tests agree with DMA outputs. Tan δ curve of ECD0.3 highlighted a predominant stiffness effect and a larger amount of hydrogen bond interactions compared to ECD0.1, due to the highest loading of CDs in the polymer matrix (Fig. 4a, section 3.3). Based on that, it appears clear that the epoxy network of ECD0.3 shows higher reversibility than that of ECD0.1. These FTSR tests better elucidate the synergistic action of both types of CDs. The functionalized nanoparticles confined at the surface of epoxy nanocomposites prevent the flaming combustion of the samples during the reshaping, also slowing down the heat transfer to the first layers of polymer, while the CDs located throughout the matrix enable the shape recovery thanks to the dynamic reversibility of multiple hydrogen bonds. The FTSR of ECD0.1 and ECD0.3 was performed three times, after programming them in the same temporary bent shape before the start of each test. Fig. 6 displays that three FTSR cycles carried out on the same samples (see ECD0.1-3R and ECD0.3-3R in Fig. 6b) do not show any residual char formed on their surface, which still appear transparent and structurally intact. These results demonstrate the outstanding and unique capability of epoxy nanocomposites containing CDs (even at very low loadings) to combine very low surface flammability with shape recovery features.

DMA measurements were performed to investigate the effect of flame-triggered shape recovery on the viscoelastic response, as a function of temperature, of epoxy nanocomposites. ECD0.1-1R, ECD0.3-1R, ECD0.1-3R, and ECD0.3-3R exhibit slightly sharper tan δ curves (Fig. 7a and 7b) compared to ECD0.1 and ECD0.3. The FTSR of epoxy nanocomposites makes these materials more similar to the pristine resin, reducing their elastic behavior and increasing their ability to dissipate energy received from a load application [62]. However, the FTSR process does not significantly affect the mobility of epoxy chains, as the Tg values of ECD0.1-1R, ECD0.3-1R, ECD0.1-3R, and ECD0.3-3R are almost the same as those of the pristine samples (Fig. 7a and 7b). Fig. 7c and 7d display the storage moduli measured as a function of the temperature for ECD0.1, ECD0.3, and the above-said samples. After one FTSR cycle, ECD0.1 and ECD0.3 exhibit a slight decrease in the values of E' in the glassy state region, with respect to the original nanocomposites. On the other hand, unlike ECD0.3, ECD0.1 after three FTSR cycles shows higher E' values compared to the original sample. Regardless of the amount of CDs, with the advance of FTSR cycles, progressive strengthening of the materials occurs during their plastic deformation [21,63]. The heat provided during the FTSR of ECD0.1 and ECD0.3 may induce a partial condensation of hydroxyl groups on the surface of CDs and, as a consequence, their aggregation [64]. This phenomenon, together with the partial volatilization of acetone and water, may reduce the free volume between packed polymer chains and cause a hindering effect in the epoxy network. The strengthening effect stemming from the repeated application of FTSR on epoxy nanocomposites appears evident looking at the flexural modulus (E_f) and bending stress (σ_f) values

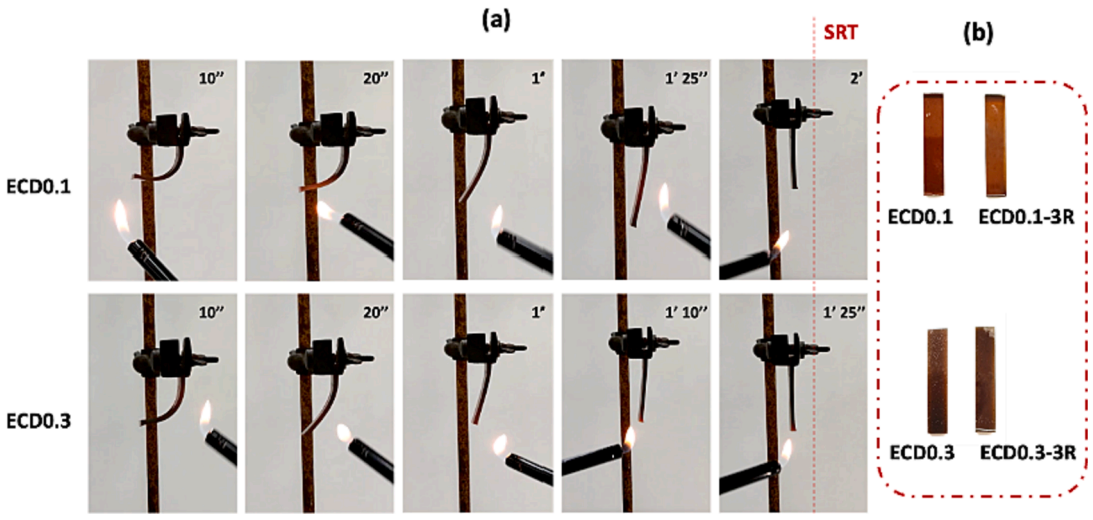

Fig. 6. Snapshots taken during flame-triggered shape recovery tests for ECD0.1 and ECD0.3 sample, including their SRT (a). The samples, at the end of three flame-triggered shape recovery cycles, do not exhibit any residual char on their surface (b).

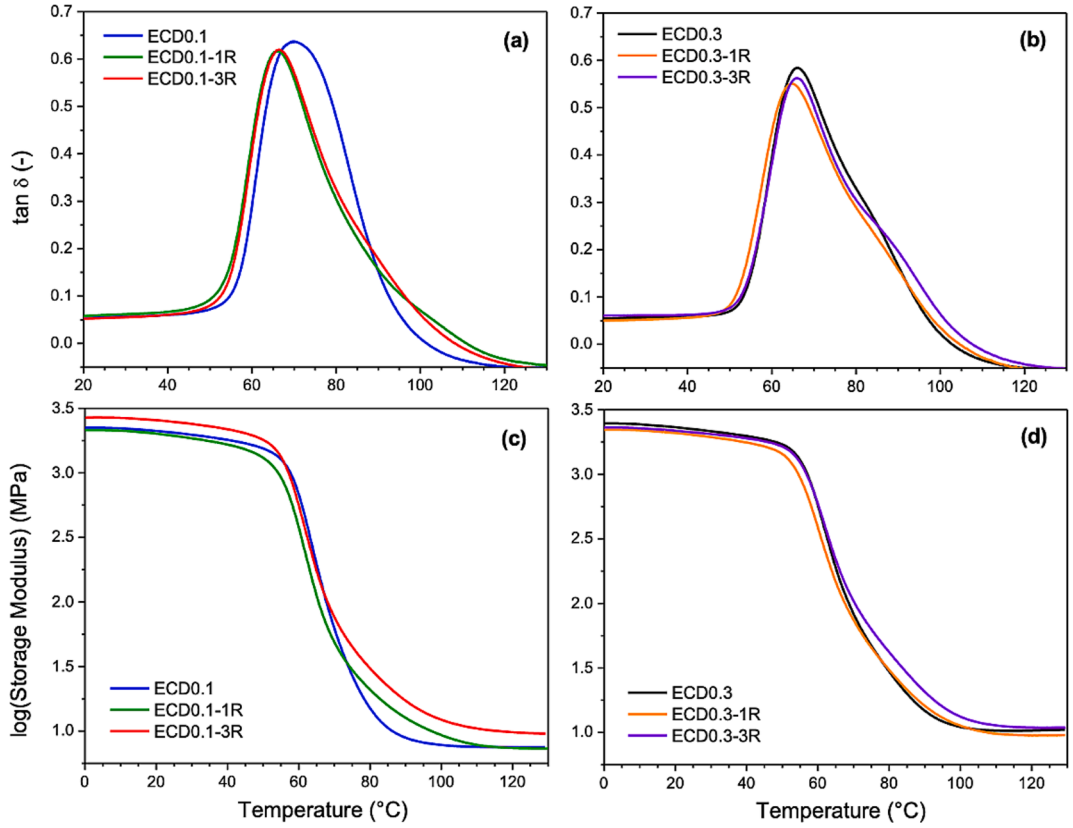

Fig. 7. Tan δ vs. temperature curves for pristine epoxy nanocomposites, and one time and three times flame-triggered shape-recovered samples (a, b). Storage moduli (E′) vs. temperature curves for the same specimens (c, d).

obtained from three-point bending tests and collected in Table 3. The standard deviation and the 95 % confidence interval of the mean value, C.I. of these mechanical parameters, were calculated following the ISO 2602 standard [65]. All the tests were performed up to 5 % of strain without any breakage, except for a couple of ECD0.3 samples that showed a quite brittle behavior.

First, it is noteworthy that the application of FTSR cycles causes a reduction in the stiffness of samples for both the epoxy nanocomposites containing CDs compared to the pristine counterparts. More specifically, a single recovery cycle provides a decrease in the elastic modulus of about 31 % and 17 %, while three cycles result in a drop of 7 % and 12 %, respectively for ECD0.1 and ECD0.3 (Table 3). Conversely, no significant differences in terms of bending stress were observed from the tests carried out on ECD0.3, although the resulting standard deviation was higher than that observed for ECD0.1 specimens. Finally, in agreement with DMA results, the specimens subjected to three FTSR cycles (namely, ECD0.1-3R and ECD0.3-3R) exhibit higher E_f and σ_f at 5 % strain with respect to ECD0.1-1R and ECD0.3-1R, further confirming

the progressive strengthening of the nanocomposites during their plastic deformation.

To investigate the thermal stability of FTSR epoxy nanocomposites, thermogravimetric analyses of ECD0.1-3R and ECD0.3-3R were performed under N_2. Fig. S5 displays that the shape recovery process does not affect the pyrolytic decomposition profile of epoxy nanocomposites, which still appears similar to that of typical aliphatic epoxy systems [66,67]. However, Table 2 shows that ECD0.1-3R and ECD0.3-3R samples decompose at higher temperatures compared to the as-prepared counterparts (see the increase in $T_{5\%}$ and $T_{10\%}$ and residue at T_{max}), giving rise to the formation, at the same time, of a higher residual char. Based on these results, it seems that the FTSR of epoxy nanocomposites enhances the thermal stability of the polymer matrix, possibly due to the flame treatment that increases the graphitization of functionalized CDs [68–70]. As regards ECD0.1-3R and ECD0.3-3R, this graphitization effect at the surface of nanocomposites significantly slows down the heat exchange at the boundary layer, and in combination with a more rigid epoxy network postpones the occurrence of decomposition phenomena even more than in the case of the pristine samples (Table 2).

3.6. Fire behavior of epoxy nanocomposites containing carbon dots

To assess the suitability of ECD0.1 and ECD0.3 to be used as fire protective coatings, the burn-through resistance was assessed by a homemade test. The configuration and methodology followed to carry out the burn-through test is depicted in Scheme S1. The fire response to the burn-through of epoxy nanocomposites was compared with the one of pristine resin. The flame tip of a gas blowpipe was applied to the middle of the sample surface till this latter lost its structural integrity (i.e., highlighting the formation of visible cracks or holes throughout the epoxy matrix) [71]. The burn-through test was carried out by using an IR camera to record the back temperature (T_B) profile at the sample surface during the flame application. Fig. 8 shows the back temperature profile along time for E, ECD0.1, and ECD0.3, together with the IR-images of the samples captured at different selected times. Burn-Through time (BTT) represents the time, at which the material loses its structural integrity.

When the flame tip of the gas blowpipe is applied to the surface of the material, it starts to decompose releasing flammable gases mixing with oxygen. As the test is performed by continuously applying the flame, the sample captures the flame when the time to ignition and the lower flammability limit in the gas phase are achieved. The flaming combustion of samples and the loss of their structural integrity are strongly dependent on the heat transfer phenomena taking place at the surface of the tested materials. Fig. 8 shows that the addition of CDs into the epoxy matrix notably increased the TTI (i.e., the time required by the sample to capture the flame and start its flaming combustion) up to ~ 150 % compared to that of the unfilled epoxy sample. In particular, the flaming combustion of ECD0.3 started only when T_B was equal to 51 °C, while the unfilled resin already captured the flame at 40 °C. Also, E lost its structural integrity at a T_B of around 140 °C, when ECD0.1 and ECD0.3 still appeared perfectly intact. It is worth mentioning that the T_B of ECD0.3 rose up to 140 °C very slowly with respect to those of unfilled resin and ECD0.1. The time required by ECD0.3 to achieve a $T_B = 140$ °C was almost 75 % higher than those of E and ECD0.1. Based on these results, CDs demonstrate their high efficiency not only in lowering the flammability of epoxy but also the heat transfer at the sample surface, especially when their content in the matrix is 0.3 wt%. Unlike the unfilled resin, ECD0.1 and ECD0.3 lost their structural integrity after almost 1 min (burn-through time) of flame application, whereas E degraded forming a visible long crack (Fig. 8) in less than 20 s [71]. Besides, the loss of integrity for ECD0.1 and ECD0.3 occurred at a T_B about 62 % higher than E. The back temperature profiles of ECD0.1 and ECD0.3 change their slope at T_B around 200 °C (Fig. 8), probably due to the thermal features of aliphatic epoxy networks, which usually start to decompose hardener-containing moieties in a temperature range between 200 and 350 °C (see section 3.3). This could explain the low T_B value (140 °C), at which the E sample lost its structural integrity compared to ECD0.1 and ECD0.3 (T_B values of 349 and 367 °C, respectively), where the presence of highly graphitized CDs lowers the heat transfer at the surface [72,73], fostering the production of an abundant amount of char (Fig. S6), able to act as thermal insulator and oxygen barrier. Silane-functionalized CDs at the surface of the epoxy nanocomposites exert their flame retardant action through the above-mentioned condensed phase mechanisms during the first stages of the decomposition process: therefore, they are highly suitable to be used as

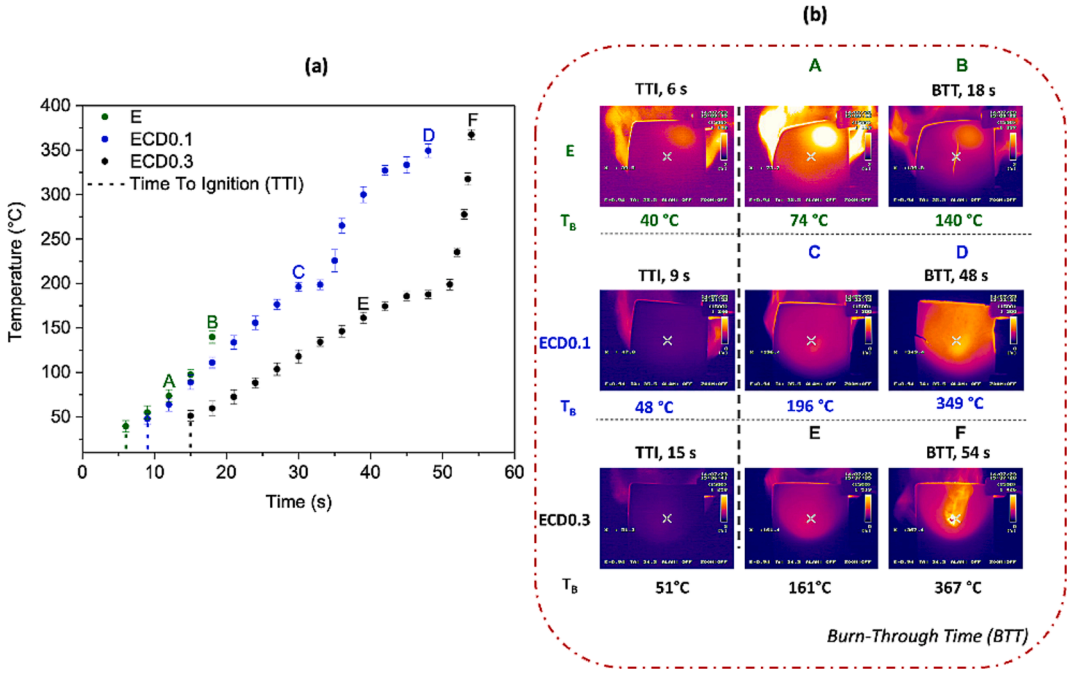

Fig. 8. Back temperature (T_B) profiles along time collected for E, ECD0.1, and ECD0.3 (a), and IR images of the samples captured at different times during burn-through tests (b).

filler in the manufacturing of fire protective coatings showing very low flammability, remarkable resistance to burn-through and high thermal insulating performances.

To investigate the fire behavior of pristine resin and epoxy nanocomposites, cone calorimetry (CC) tests were performed to evaluate different fire and smoke parameters. The volatiles are produced by exploiting a heat radiation source and their ignition is triggered by a spark [27,74]. To highlight the main flame retardant features resulting from the use of functionalized CDs, the cone calorimetry tests were performed only on pristine resin and ECD0.3, as this sample was proven to have the lowest flammability and the best thermal insulating performances (see above). CC data are summarized in Tables 4 and 5; Fig. 9 shows the related Heat Release Rate (HRR) vs. time curves for E and ECD0.3 samples. The combustion of unmodified resin and epoxy nanocomposite occurs following similar HRR profiles along time, therefore it is likely that CDs do not deeply affect the fire behavior of epoxy in terms of heat released. However, the incorporation (at 0.3 wt%) of CDs into the epoxy matrix leads to a slight decrease (14 %) in HRR compared to the virgin resin. On the other side, ECD0.3 exhibits lower TTI and Total Heat Release (THR) values than E (Table 4), due to the acidic characteristics of CDs, which promote the dehydration of polymer matrix and in turn boost the char formation during the combustion [72,75].

With respect to E, ECD0.3 shows a lower CO/CO_2 ratio, together with an increase of the residual mass obtained from CC tests, confirming that the flame retardant mechanism takes place in the condensed phase of the epoxy nanocomposite (Tables 4 and 5).

SEM analysis of the chars resulting from CC tests of E and ECD0.3 (Fig. 10) shows that the combustion of pristine resin produces a carbonaceous residue characterized by a loose morphology, full of cracks and holes, compared to that obtained from the epoxy nanocomposite, which appears very compact and continuous. Also, SEM-EDX results highlight a significant retention of Si in the residual char of ECD0.3 (Fig. 10), suggesting the presence of Si-O-Si polymeric substructures (yellow balls in Fig. 9), formed through condensation reactions between silicon-containing moieties of HDTMS and hydroxyl groups on the surface of CDs. This hybrid char deriving from the combustion of ECD0.3 can strongly limit the heat exchange and the oxygen diffusion between the gas phase and the polymer matrix, acting as an effective ceramic thermal shield during the combustion of the epoxy nanocomposite (Fig. 9). The residual chars of E and ECD0.3 were also analyzed by FTIR (Fig. 10). In the spectra of the char of ECD0.3 sample, peaks at 638 cm^{-1}, 802 cm^{-1}, and 871 cm^{-1} are ascribed to aromatic C–H vibrations in meta, para, and ortho, respectively [76,77]. The presence of such peaks and the disappearance of the band at 1226 cm^{-1}, due to oxygenated species (e.g., phenol, 4-isopropylphenol), proves that this char contains more aromatic structures compared to that of pristine resin. Also, the C = C stretching vibration at 1577 cm^{-1}, combined with the low intensity of the band at 3430 cm^{-1} linked to O–H stretching vibration, gives evidence of carbonization via dehydration of epoxy resin by CDs [46,78]. These charring phenomena also occur during the combustion of the unfilled resin, although they appear much more relevant in the case of the epoxy nanocomposite [8,79]. Finally, the Si–O–Si stretching vibration band at 1086 cm^{-1} confirms the presence of silicon-based polymeric substructures in the char formed from the combustion of ECD0.3, further supporting the generation of a hybrid ceramic char [46,80].

The characteristic morphology of this silicon-containing char and its effective thermal shielding effect, together with the charring behavior of the functionalized CDs (Type II of Fig. 5, section 3.4), mainly located at the surface of the epoxy nanocomposite, are responsible for the very low surface flammability and high thermal insulating performances. As confirmed by CC and burn-through results, the flame retardant action of functionalized CDs is particularly effective in improving the fire resistance of the surface, while the bulk properties and thus the fire behavior of epoxy nanocomposites are not significantly affected. Besides, the excellent distribution of graphitized CDs and their small size (section 3.1) make them able to exert their flame retardant mechanism in the condensed phase during the first combustion stages [72,81], resulting in an outstanding beneficial effect on the smoke parameters (i.e., TSR and SEA) of ECD0.3, which are very low compared to those of E (Table 5) [82]. The slowdown of the heat exchange phenomena at the surface of nanocomposites causes a delayed production of smoke, as this latter is mainly composed of several aromatic compounds (e.g., benzene, naphthalene), which form during the last stages of the carbonization and gas-phase combustion processes at high temperatures (i.e., 800–1000 °C). The implementation of new materials able to reduce smoke emissions is highly desirable in the manufacturing of new technologies, as it minimizes the risk to human lives and helps the firemen during evacuations. The strategy proposed in this research work may represent a valuable methodology to obtain transparent fire protective coatings based on aliphatic epoxy nanocomposites, showing sustainable features, and using very low loadings (i.e., up to 0.3 wt%) of carbonaceous biowaste-derived functional filler. Also, this strategy does not involve the use of any halogen or phosphorus-based flame retardant, avoiding depletion of natural resources or the release of possible toxic species, even allowing for the achievement of unprecedented surface fire resistance [27,74].

Table 5
Smoke parameters from cone calorimetry tests for the investigated samples.

Sample	TSR (m^2/m^2)	ΔTSR (%)	SEA (m^2/kg)	ΔSEA (%)	CO yield (kg/kg)	CO_2 yield (kg/kg)	CO/CO_2
E	2428 ± 208	–	910 ± 35	–	0.016 ± 0.003	0.04 ± 0.06	0.4
ECD0.3	1451 ± 216	−40	812 ± 30	−11	0.076 ± 0.003	0.34 ± 0.05	0.2

TSR = Total Smoke Release, SEA = Specific Extension Area.

3.7. Anticounterfeiting features of the epoxy nanocomposites containing carbon dots for packaging applications

Counterfeiting is one of the major concerns that poses significant hurdles to consumers and businesses alike. Damages to brand reputation, troubles to consumer safety, and economic losses are some of the issues linked to the increase of counterfeit products [83]. To face these issues, various anti-counterfeiting strategies and solutions have been developed. Unique identification technologies are usually categorized into logical security, such as IDs, and physical security, such as holograms and others [84,85]. Logical security on a product can be easily copied, as the protection method is based on the storage of the IDs in a database. Conversely, physical security on the product itself is much more difficult to copy, although it often provides no uniqueness to it, with respect to the logical security [86].

The use of the epoxy nanocomposites proposed in this research work may provide uniqueness to the product or its polymer-based packaging, as it would allow for incorporating a distinctive element, composed of a transparent sensing material, showing properties (i.e., hydrophobicity,

Table 4
Results from cone calorimetry tests for the investigated samples.

Sample	TTI (s)	TTFO (s)	THR (MJ/m^2)	ΔTHR (%)	HRR (kW/m^2)	ΔHRR (%)	pkHRR (kW/m^2)	Residue (wt.%)
E	46 ± 3	208 ± 3	81 ± 3	–	294 ± 23	–	1431 ± 62	2 ± 0.7
ECD0.3	44 ± 1	192 ± 0.5	67 ± 2	−17	252 ± 21	−14	1450 ± 81	4 ± 0.5

TTI = Time To Ignition, TTFO = Time To Flame Out, THR = Total Heat Release, HRR = Heat Release Rate, pkHRR = peak of Heat Release Rate.

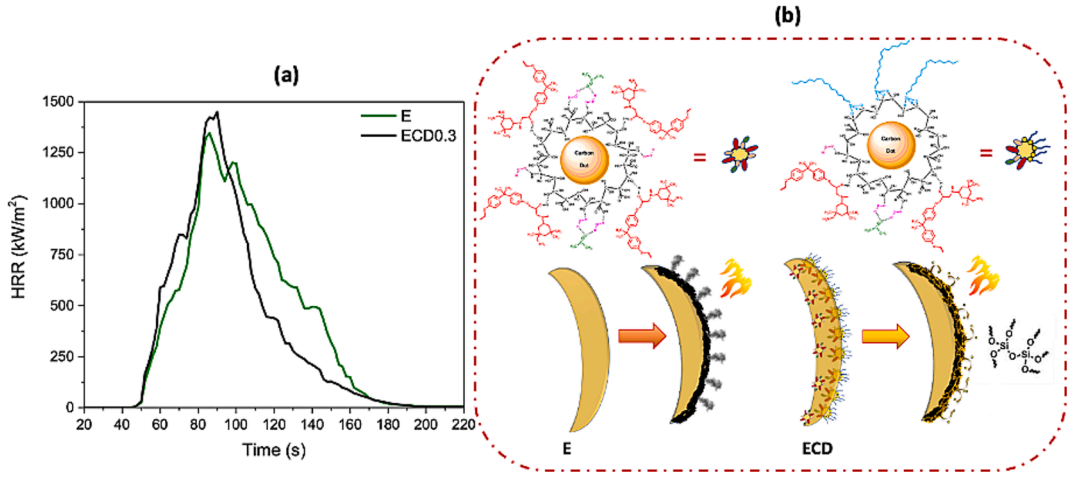

Fig. 9. Heat release rate (HRR) vs. time of pristine resin and the epoxy nanocomposite containing 0.3 wt% of carbon dots (a). Possible flame retardant mechanisms involved (b).

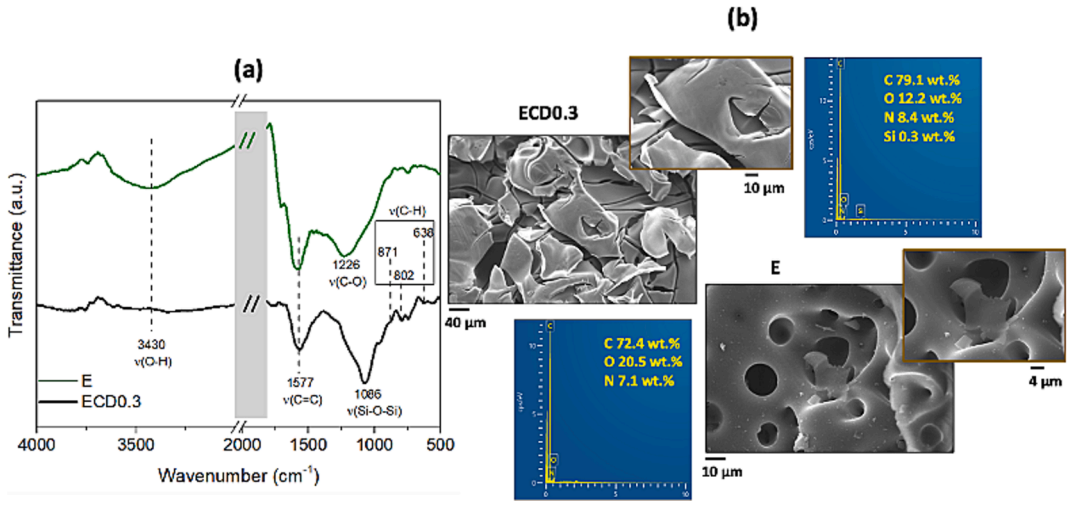

Fig. 10. FTIR spectra (a) and SEM-EDX images (b), with related abundances, of chars after cone calorimetry test carried out on pristine resin and the epoxy nanocomposite containing 0.3 wt% of carbon dots.

photoluminescence, fire resistance, heat/flame-triggered shape recovery), which are very difficult to copy or implement in a single material. In addition to anti-counterfeiting opportunities, the application of the epoxy nanocomposites containing CDs on packaging polymers would reduce the flammability and improve thermal insulating performances of this no-charring and very flammable plastic [87], leading to several benefits in terms of fire safety. Polypropylene (PP) was selected as representative of polymers used for packaging applications [88,89], as it is largely employed thanks to very good barrier qualities, excellent strength, and superior surface quality at low cost. PP can be blow-molded or thermoformed to create different packaging shapes for items like personal care products, medical apparatuses, and food. To test the suitability of epoxy nanocomposites as protective coatings for packaging applications, ECD0.1 was applied on PP films, and its performances in terms of hydrophobicity, flame retardancy, and shape recovery were evaluated.

3.7.1. Hydrophobic polypropylene substrates coated by epoxy nanocomposites containing CDs

To test the hydrophobicity of PP films coated by pristine resin and epoxy nanocomposites, the substrates were clamped to rectangular polystyrene support (Fig. S7). The surface of PP substrate was separated into three sections (10 × 20 × 0.2 mm^3): one uncoated, and the other two respectively coated by E and ECD0.1. Based on the flammability results, five layers (thickness ~ 300 µm) of both epoxy systems (E and ECD0.1) were deposited with a brush and cured following the procedure reported in section 2.4. The deposition of these coatings did not cause any change in the transparency of the PP substrate. Then, water drops of volume in the range of 30–40 µL were placed on each section. Fig. S7 shows that the water contact angle increased moving from pure PP to the section treated by the resin, which is due to the more hydrophobic character of epoxy compared to the polyolefin. However, the use of ECD0.1 as coating material guaranteed the highest water contact angle, demonstrating the establishment of a unique property on the surface of the PP film. This new feature of treated PP may be used to protect the authenticity of commercial packaging. Besides, PP-based packaging can easily swell, therefore the application of ECD0.1 may prevent its deterioration caused by the absorption of moisture during the transportation or storage of products.

3.7.2. Flammability of polypropylene substrates coated by epoxy nanocomposites containing CDs

To test their flammability, PP films treated with pristine resin and epoxy nanocomposites containing CDs were used as substrates and their

surfaces were separated into three sections (100 × 20 × 0.2 mm^3): one uncoated, and the other two respectively coated by E and ECD0.1. E and ECD0.1 were deposited and cured by following the procedure reported in section 2.4. The PP film was fixed by a holding clamp to a metal support, which was placed under a fume cupboard, switching off the aspiration during the test (Fig. 11a).

The flame tip of a gas lighter was applied to all three coated sections of the PP substrate and the response of the material was recorded. As previously mentioned, PP is a highly flammable no-charring polymer, therefore its combustion does not produce carbonaceous residue, but combustible gases released in the gas phase. According to the U.S.-based National Fire Protection Association, PP belongs to the fire hazard classification of four, owing to its high flammability [90,91]. The low melting point of PP, ranging from 145 to 195 °C, limits its applications to some fields, also including packaging. The large diffusion of PP-based packaging makes the improvement of its fire behavior an important requirement. The application of the flame to the uncoated section of the PP substrate caused its melting and slight combustion, with a little char residue left on the surface of the material, in less than 1 s (Fig. 11a, Video 4) [27,92]. Similar results were obtained by applying the flame to the sections coated by one layer (thickness ~ 60 μm) of E or ECD0.1. However, the deposition of a minimum number of five layers (thickness ~ 300 μm) on the PP substrate was able to slow down the occurrence of decomposition phenomena up to more than 5 s (Fig. 11a, Video 5). The section of PP film coated by five layers of ECD0.1 did not show any deterioration or color change after the flame application. Conversely, the flammability tests performed on the section of PP film coated by five layers (thickness ~ 300 μm) of E gave rise to the same result (see Video 6) observed in the case of one layer. The thermal insulating feature and good fire behavior of the epoxy nanocomposite lowered the heat transfer and flammability of the PP substrate, imparting not only an additional unique property to the packaging material but also more fire safety characteristics.

3.7.3. *Flame-triggered shape recovery of polypropylene substrates coated by epoxy nanocomposites containing CDs*

PP films coated by epoxy nanocomposites containing CDs could be programmed in a temporary shape. The application of a flame to such coated PP films could trigger the recovery of their original shape. The possibility to change the shape geometry of polymeric materials may reduce the amount of plastic waste, as the end-of-life polymer-based product may be reused for a new application. On the other side, the incorporation in the commercial packaging of elements able to recover their shape by a stimulus, such as a flame, may offer the possibility of a unique identification technology for the authenticity protection of genuine items.

To test the flame-triggered shape recovery capability of PP films coated by ECD0.1, their surface was separated into three sections (100 × 20 × 0.2 mm^3): one located in the middle of the sample and coated by ECD0.1 (Fig. 11b), and the other two both uncoated. Five layers (thickness ~ 300 μm) of ECD0.1 were deposited with a brush and the PP film was fixed in a double bent shape, before being cured as reported above (section 2.4), thus making this the original or permanent shape. The flame-triggered shape recovery of the double-bent PP film coated by ECD0.1 was tested through a configuration similar to the one used for evaluating the flammability of treated PP substrates (Fig. 11a). As regards the programming step, the flame tip of a gas lighter was applied to the section of the double-bent PP film coated by ECD0.1 till the sample acquired a temporary flat shape (Fig. 11b). After the flame application, the temporary flat shape was definitely established by keeping a load at the bottom of the PP film and keeping constant the strain during its cooling to room temperature (~27 °C). The original double-bent shape of the PP film could be recovered by applying the flame to the section coated by ECD0.1 (recovering step) and then cooling the sample to room temperature without the use of any external force (e.g., load). Fig. 11b shows that the flame-triggered shape recovery of PP film did not affect its transparency nor cause any decomposition phenomenon and char formation.

It was demonstrated that the epoxy nanocomposite containing carbon dots can be applied as a coating on PP films, conferring unique functionalities to the commercial polyolefin substrate. Based on that, the investigated nanocomposites may be considered for the manufacturing of unique identification technologies, paving the way to differentiate genuine products and their packaging from counterfeits. Also, the methodology implemented in this research work may be used to obtain shape-recovery polymers for the preparation of smart composites with a biowaste-derived functional filler.

4. Conclusions

Carbon dots (CDs) represent a valid alternative to the conventional inorganic semiconductor quantum dots to design and prepare aliphatic

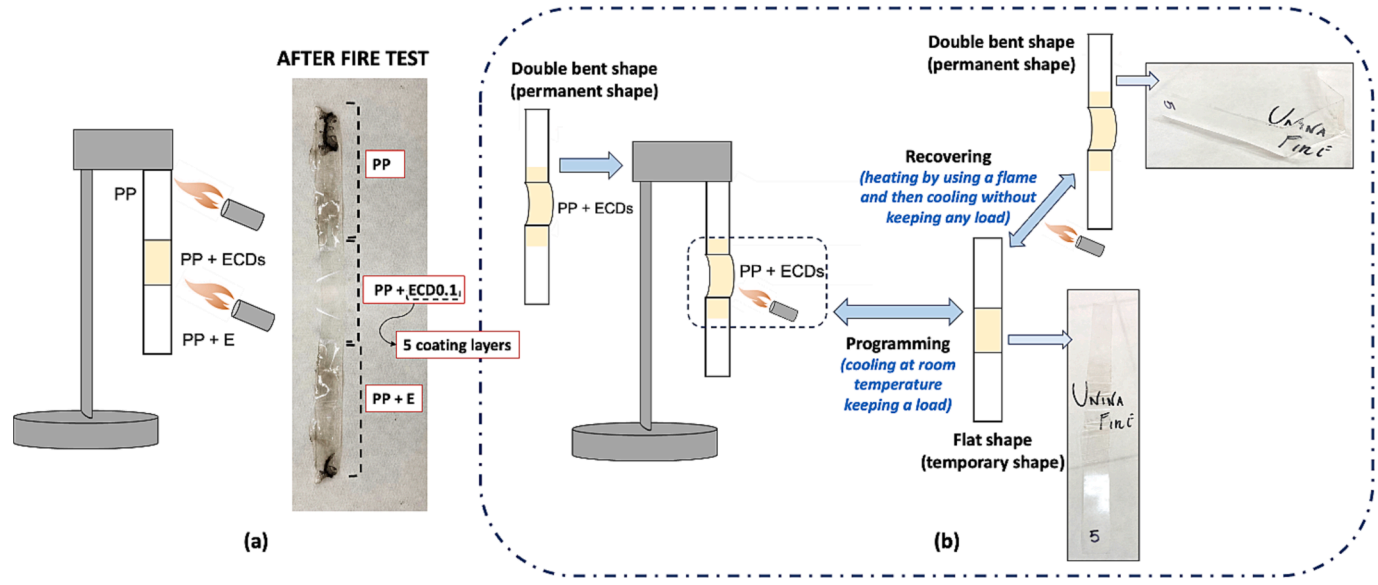

Fig. 11. Flammability tests performed on polymeric films made of polypropylene (PP) (a). Schematic representation of the flame-triggered shape recovery process of PP films coated by epoxy nanocomposites (b).

DGEBA-based epoxy nanocomposites showing photoluminescence and sensing features. Here, we demonstrated that CDs can be used alone, without any flame retardant additive or chemical modification of the polymer matrix, for the preparation of thermosetting nanocomposites showing not only transparency and photoluminescence but also high hydrophobicity, an intriguing heat/flame-triggered shape recovery behavior, and very low flammability as well as smoke emissions. This multifunctionality is due to the graphitic nature and surface chemistry of these CDs, obtained from a renewable source such as humic acid, which makes them a perfect platform for further functionalization. The proposed design and synthesis strategies are based on the use of minimal amounts (0.1, 0.3 wt%) of CDs together with a sustainable alkylsilane. The interactions between CDs and silane molecules enable the carbonaceous nanostructures to locate at the surface, and their synergistic effects allow for the fabrication of epoxy nanocomposites exhibiting fire-resistant, poor thermally conductive, and almost superhydrophobic surfaces, keeping good mechanical performances after the flame-triggered shape recovery process. As highlighted by burn-through tests, thermosets containing CDs accounted for increased ignition times (up to ~ 150 %) and about three times higher burn-through times, with respect to the unfilled epoxy.

Nowadays, the demand for new low-cost easy-to-prepare multifunctional materials with extendable lifetimes and high performances is constantly growing. The use of CDs may offer an extremely advantageous solution, as their size, structure, and surface chemistry can be tailored and adapted to the needs of specific applications. These nanomaterials allow for the synthesis of thermosetting nanocomposites, also suitable to be employed as coatings, paving the way for the preparation of more functional and sustainable technologies, which could be implemented for the manufacturing of anti-counterfeiting tools, fire-resistant lightening items, and flexible geometry sensors for 5G communication.

CRediT authorship contribution statement

Aurelio Bifulco: Writing – original draft, Validation, Methodology, Investigation, Formal analysis, Conceptualization. **Claudio Imparato:** Writing – review & editing, Methodology, Investigation, Formal analysis, Conceptualization. **Immacolata Climaco:** Visualization, Investigation, Formal analysis. **Daniele Battegazzore:** Investigation, Formal analysis. **Michele Perrella:** Writing – review & editing, Methodology, Investigation, Formal analysis. **Giuseppe Vitiello:** Writing – review & editing, Methodology, Investigation, Formal analysis, Conceptualization. **Antonio Aronne:** Writing – review & editing, Validation, Supervision, Resources, Funding acquisition. **Giulio Malucelli:** Writing – review & editing, Validation, Supervision, Methodology, Conceptualization.

Declaration of competing interest

The authors declare that they have no known competing financial interests or personal relationships that could have appeared to influence the work reported in this paper.

Data availability

Data will be made available on request.

Acknowledgements

Dr. Aurelio Bifulco acknowledges the Italian Ministry of Education and Research, PON R&I 2014-2020 – Asse IV "Istruzione e ricerca per il recupero – REACT-EU" – Azione IV.6 – "Contratti di ricerca su tematiche Green", for the financial support concerning his employment contract. The authors are grateful to Philip Morris International and CeSMA (Centro Servizi Metrologici e Tecnologici Avanzati – University of Naples Federico II) for the financial support related to the employment contract (research scholarship) to Ms. Immacolata Climaco.

Appendix A. Supplementary data

Supplementary data to this article can be found online at https://doi.org/10.1016/j.cej.2024.149327.

References

[1] L. Vertuccio, L. Guadagno, G. Spinelli, P. Lamberti, M. Zarrelli, S. Russo, G. Iannuzzo, Smart coatings of epoxy based CNTs designed to meet practical expectations in aeronautics, Compos. b. Eng. 147 (2018) 42–46.
[2] G. Cricrì, M. Perrella, V.P. Berardi, Identification of cohesive zone model parameters based on interface layer displacement field of bonded joints, Fatigue Fract. Eng. Mater. Struct. 45 (3) (2022) 821–833.
[3] W. Post, A. Susa, R. Blaauw, K. Molenveld, R.J.I. Knoop, A review on the potential and limitations of recyclable thermosets for structural applications, Polymer Rev. 60 (2) (2020) 359–388.
[4] H. Memon, Y. Wei, C. Zhu, Recyclable and reformable epoxy resins based on dynamic covalent bonds–Present, past, and future, Polym. Test. 105 (2022) 107420.
[5] V. Chauhan, T. Kärki, J. Varis, Review of natural fiber-reinforced engineering plastic composites, their applications in the transportation sector and processing techniques, J. Thermoplast. Compos. Mater. 35 (8) (2022) 1169–1209.
[6] Z. Fan, I. Noh, C. Zhuang, Q. Liu, Y. Wang, H. Do Kim, M. Yue, H. Ohkita, B. Wang, A polar polyimide as multifunctional flame retardant for epoxy resin through constructing intimate 3D interpenetrating polymer network, Eur. Polym. J. (2023) 112383.
[7] Y. Wang, E.C. Alocilja, Sensor technologies for anti-counterfeiting, I Int, J. Comp. Appl. Crim. Justice 36 (4) (2012) 291–304.
[8] B.W. Liu, H.B. Zhao, Y.Z. Wang, Advanced flame-retardant methods for polymeric materials, Adv. Mater. 34 (46) (2022) 2107905.
[9] S. Hörold, Phosphorus flame retardants in thermoset resins, Polym. Degrad. Stabil. 64 (3) (1999) 427–431.
[10] W.W. Klingler, A. Bifulco, C. Polisi, Z. Huang, S. Gaan, Recyclable inherently flame-retardant thermosets: Chemistry, properties and applications, Compos. b. Eng. 258 (2023) 110667.
[11] K. Wang, X. Liu, Y. Dong, Z. Ling, Y. Cai, D. Tian, Z. Fang, J. Li, Editable shape-memory transparent wood based on epoxy-based dynamic covalent polymer with excellent optical and thermal management for smart building materials, Cellul. 29 (14) (2022) 7955–7972.
[12] S.Y. Lim, W. Shen, Z. Gao, Carbon quantum dots and their applications, Chem. Soc. Rev. 44 (1) (2015) 362–381.
[13] J. Wu, T. Chen, S. Ge, W. Fan, H. Wang, Z. Zhang, E. Lichtfouse, T. Van Tran, R. K. Liew, M. Rezakazemi, Synthesis and applications of carbon quantum dots derived from biomass waste: a review, Environ. Chem. Lett. 21 (6) (2023) 1–32.
[14] F. Salehtabar, M. Ghaemy, Preparation of strongly photoluminescent nanocomposite from DGEBA epoxy resin and highly fluorescent nitrogen-doped carbon dots, Polym. Bull. 80 (3) (2023) 3247–3264.
[15] U. Lee, E. Heo, T.-H. Le, H. Lee, S. Kim, S. Lee, H. Jo, H. Yoon, Carbon dots for epoxy curing: Anti-forgery patterns with long-term luminescent stability, Chem. Eng. J. 405 (2021) 126988.
[16] H. Liu, F. Wang, W. Wu, X. Dong, L. Sang, 4D printing of mechanically robust PLA/TPU/Fe3O4 magneto-responsive shape memory polymers for smart structures, Compos. b. Eng. 248 (2023) 110382.
[17] S. Basak, A. Bandyopadhyay, Solvent Responsive Shape Memory Polymers-Evolution, Current Status, and Future Outlook, Macromol. Chem. Phys. 222 (19) (2021) 2100195.
[18] H. Zheng, S. Wang, C. Lu, Y. Ren, Z. Liu, D. Ding, Z. Wu, X. Wang, Y. Chen, Q. Zhang, Thermal, near-infrared light, and amine solvent triple-responsive recyclable imine-type vitrimer: shape memory, accelerated photohealing/welding, and destructing behaviors, Ind. Eng. Chem. Res. 59 (50) (2020) 21768–21778.
[19] Y. Liu, J. Zhao, L. Zhao, W. Li, H. Zhang, X. Yu, Z. Zhang, High performance shape memory epoxy/carbon nanotube nanocomposites, ACS Appl. Mater. Interfaces 8 (1) (2016) 311–320.
[20] W. Zhao, C. Yue, L. Liu, Y. Liu, J. Leng, Research progress of shape memory polymer and 4D printing in biomedical application, Adv. Healthc. Mater. 12 (16) (2023) 2201975.
[21] A. Yadav, S.K. Singh, S. Das, S. Kumar, A. Kumar, Shape recovery and mechanical properties investigation of carbon fiber dispersed bisphenol-A based epoxy composite, Smart Mater. Struct. 32 (9) (2023) 95016.
[22] L. Guadagno, L. Vertuccio, C. Naddeo, E. Calabrese, G. Barra, M. Raimondo, A. Sorrentino, W.H. Binder, P. Michael, S. Rana, Self-healing epoxy nanocomposites via reversible hydrogen bonding, Compos. b. Eng. 157 (2019) 1–13.
[23] A. Campanella, D. Döhler, W.H. Binder, Self-healing in supramolecular polymers, Macromol. Rapid Commun. 39 (17) (2018) 1700739.
[24] F. Herbst, D. Döhler, P. Michael, W.H. Binder, Self-healing polymers via supramolecular forces, Macromol. Rapid Commun. 34 (3) (2013) 203–220.
[25] C. Lu, Z. Ling, C. Wang, J. Wang, Q. Yong, F. Chu, Multiple hydrogen bonding interactions toward rapidly self-healing, photothermal conversion elastomer composites, Compos. b. Eng. 228 (2022) 109428.

[26] S. Mathew, B. Mathew, A Review on the Synthesis, Properties, and Applications of Biomass Derived Carbon Dots, Inorg. Chem. Commun. 156 (2023) 111223.
[27] X. Feng, J. Fan, A. Li, G. Li, Multireusable Thermoset with Anomalous Flame-Triggered Shape Memory Effect, ACS Appl. Mater. Interfaces 11 (17) (2019) 16075–16086.
[28] J. Passaro, A. Bifulco, E. Calabrese, C. Imparato, M. Raimondo, R. Pantani, A. Aronne, L. Guadagno, Hybrid Hemp Particles as Functional Fillers for the Manufacturing of Hydrophobic and Anti-icing Epoxy Composite Coatings, ACS Omega 8 (26) (2023) 23596–23606.
[29] D.K. Owens, Some thermodynamic aspects of polymer adhesion, J. Appl. Polym. Sci. 14 (7) (1970) 1725–1730.
[30] I.S.O. Standard, B. Iso, Plastics—Determination of flexural properties, ISO Geneva, Switzerland, 2019.
[31] A.S.T.M. Standard. Standard test methods for flexural properties of unreinforced and reinforced plastics and electrical insulating materials, ASTM D790, Annual book of ASTM Standards, 1997.
[32] Z.L. Wu, M.X. Gao, T.T. Wang, X.Y. Wan, L.L. Zheng, C.Z. Huang, A general quantitative pH sensor developed with dicyandiamide N-doped high quantum yield graphene quantum dots, Nanoscale 6 (7) (2014) 3868–3874.
[33] Y. Zhu, Y. Bao, L. Wang, J. Bi, Y. Liu, C. Xie, Hydrothermal oxidation method to synthesize nitrogen containing carbon dots from compost humic acid as selective Fe (III) sensor, Mater. Res. Express 7 (9) (2020) 095008.
[34] Y. Dong, L. Wan, J. Cai, Q. Fang, Y. Chi, G. Chen, Natural carbon-based dots from humic substances, Sci. Rep. 5 (1) (2015) 10037.
[35] W. Shi, H. Fan, S. Ai, L. Zhu, Preparation of fluorescent graphene quantum dots from humic acid for bioimaging application, New J. Chem. 39 (9) (2015) 7054–7059.
[36] T. Song, Y. Zhao, K. Matras-Postolek, P. Yang, Color-tunable carbon dots via control the degree of self-assembly in solution at different concentration, J. Lumin. 212 (2019) 69–75.
[37] A. Das, E.V. Kundelev, A.A. Vedernikova, S.A. Cherevkov, D.V. Danilov, A. V. Koroleva, E.V. Zhizhin, A.N. Tsypkin, A.P. Litvin, A.V. Baranov, Revealing the nature of optical activity in carbon dots produced from different chiral precursor molecules, Light Sci. Appl. 11 (1) (2022) 92.
[38] G. Pota, A. Bifulco, D. Parida, S. Zhao, D. Rentsch, E. Amendola, V. Califano, A. Costantini, Tailoring the hydrophobicity of wrinkled silica nanoparticles and of the adsorption medium as a strategy for immobilizing lipase: An efficient catalyst for biofuel production, Microporous Mesoporous Mater. 328 (2021) 111504.
[39] K. Koch, B. Bhushan, Y.C. Jung, W. Barthlott, Fabrication of artificial Lotus leaves and significance of hierarchical structure for superhydrophobicity and low adhesion, Soft Matter 5 (7) (2009) 1386–1393.
[40] S. Pan, A.K. Kota, J.M. Mabry, A. Tuteja, Superomniphobic surfaces for effective chemical shielding, J. Am. Chem. Soc. 135 (2) (2013) 578–581.
[41] X.-F. Zhang, X.-D. Li, N. Wang, Y.-J. Liu, F. Tian, C.-X. Wang, Robust superhydrophobic SiO2/epoxy composite coating prepared by one-step spraying method for corrosion protection of aluminum alloy: Experimental and theoretical studies, Mater Design 228 (2023) 111833.
[42] K. Li, J. Xiang, J. Zhou, X. Su, H. Xie, S. Lin, Z. Xiao, W. Huang, C. Zhao, H. Chen, Self-healing and wear resistance stable superhydrophobic composite coating with electrothermal and photothermal effects for anti-icing, Prog. Org. Coat. 177 (2023) 107415.
[43] V. Panwar, K. Pal, Dynamic mechanical analysis of clay–polymer nanocomposites, in: K. Jlassi, M.M. Chehimi, S. Thomas (Eds.), Clay-polymer nanocomposites, Elsevier, 2017, pp. 413–441.
[44] L. Mascia, L. Prezzi, M. Lavorgna, Peculiarities in the solvent absorption characteristics of epoxy-siloxane hybrids, Polym. Eng. Sci. 45 (8) (2005) 1039–1048.
[45] J. Jiao, P. Liu, L. Wang, Y. Cai, One-step synthesis of improved silica/epoxy nanocomposites with inorganic-organic hybrid network, J. Polym. Res. 20 (8) (2013) 202.
[46] A. Bifulco, R. Avolio, S. Lehner, M.E. Errico, N.J. Clayden, R. Pauer, S. Gaan, G. Malucelli, A. Aronne, C. Imparato, In Situ P-Modified Hybrid Silica-Epoxy Nanocomposites via a Green Hydrolytic Sol-Gel Route for Flame-Retardant Applications, ACS Appl. Nano Mater. 6 (9) (2023) 7422–7435.
[47] F. Wang, S. Pan, P. Zhang, H. Fan, Y. Chen, J. Yan, Synthesis and application of phosphorus-containing flame retardant plasticizer for polyvinyl chloride, Fibers Polym. 19 (5) (2018) 1057–1063.
[48] A. Bifulco, D. Parida, K. Salmeia, S. Lehner, R. Stämpfli, H. Markus, G. Malucelli, F. Branda, S. Gaan, improving flame retardancy of in-situ silica-epoxy nanocomposites cured with aliphatic hardener: combined effect of DOPO-based flame-retardant and Melamine, Compos. c: Open Access 2 (2020) 100022.
[49] D.E.C. Corbridge, The structural chemistry of phosphates, Bull. Minér. 94 (3) (1971) 271–299.
[50] R.F.M. Lange, E.W. Meijer, Supramolecular polymer interactions based on the alternating copolymer of styrene and Maleimide, Macromolecules 28 (3) (1995) 782–783.
[51] S. Yi, J. Chen, H. Li, L. Liu, X. Xiao, X. Zhang, Effect of graphite oxide on graphitization of furan resin carbon, Carbon 48 (3) (2010) 926–928.
[52] H. Luo, L. Lari, H. Kim, S. Hérou, L.C. Tanase, V.K. Lazarov, M.-M. Titirici, Structural evolution of carbon dots during low temperature pyrolysis, Nanoscale 14 (3) (2022) 910–918.
[53] S. Datta, T.C. Henry, Y.R. Sliozberg, B.D. Lawrence, A. Chattopadhyay, A.J. Hall, Carbon nanotube enhanced shape memory epoxy for improved mechanical properties and electroactive shape recovery, Polymer 212 (2021) 123158.
[54] R. Zende, V. Ghase, V. Jamdar, A review on shape memory polymers, Polym.-Plast. Technol. Mater. 62 (4) (2023) 467–485.
[55] W. Fan, Z. Li, Q. Liao, L. Zhang, L. Kong, Z. Yang, M. Xiang, Improving the Heat Resistance and Flame Retardancy of Epoxy Resin Composites by Novel Multifunctional Cyclophosphazene Derivatives, Polymers 15 (1) (2022) 59.
[56] B. Xu, W. Ma, X. Wu, L. Qian, S. Jiang, Flame retardancy and thermal behavior of intumescent flame-retardant EVA composites with an efficient triazine-based charring agent, Mater. Res. Express 5 (4) (2018) 45309.
[57] C. Liu, H. Li, R. Cheng, J. Guo, G.-X. Li, Q. Li, C.-F. Wang, X. Yang, S. Chen, Facile synthesis, high fluorescence and flame retardancy of carbon dots, J. Mater. Sci. Technol. 104 (2022) 163–171.
[58] D.M. Fox, J. Lee, C.J. Citro, M. Novy, Flame retarded poly (lactic acid) using POSS-modified cellulose. 1. Thermal and combustion properties of intumescing composites, Polym. Degrad. Stabil. 98 (2) (2013) 590–596.
[59] H. Zou, S. Wu, J. Shen, Polymer/silica nanocomposites: preparation, characterization, properties, and applications, Chem. Rev. 108 (9) (2008) 3893–3957.
[60] X. Lu, X. Gu, Fabrication of a bi-hydroxyl-bi-DOPO compound with excellent quenching and charring capacities for lignin-based epoxy resin, Int. J. Biol. Macromol. 205 (2022) 539–552.
[61] W.H. Zhao, J.W. Wang, G.C. Zhuang, D.Y. Liu, C.C. Sun, Thermal Stability and Flame Retardancy of Epoxy Resin with DOPO-Based Compound Containing Triazole and Hydroxyl Groups, Macromol. Mater. Eng. 307 (11) (2022) 2200408.
[62] J.H. Chen, J.H. Lu, X.L. Pu, L. Chen, Y.Z. Wang, Recyclable, malleable and intrinsically flame-retardant epoxy resin with catalytic transesterification, Chemosphere 294 (2022) 133778.
[63] S. Deboeuf, L. Ducloué, N. Lenoir, G. Ovarlez, A mechanism of strain hardening and Bauschinger effect: shear-history-dependent microstructure of elasto-plastic suspensions, Soft Matter 18 (46) (2022) 8756–8770.
[64] A. Bifulco, F. Tescione, A. Capasso, P. Mazzei, A. Piccolo, M. Durante, M. Lavorgna, G. Malucelli, F. Branda, Effects of post cure treatment in the glass transformation range on the structure and fire behavior of in situ generated silica/epoxy hybrids, J. Sol-Gel Sci. Technol. 87 (1) (2018) 156–169.
[65] M. Nachman, K. Kwiatkowski, The effect of thermal annealing on the abrasion resistance of a segmented block copolymer urethane elastomers, Wear 306 (1–2) (2013) 113–118.
[66] O. Zabihi, M. Aghaie, K. Zare, Study on a novel thermoset nanocomposite form DGEBA–cycloaliphatic diamine and metal nanoparticles: thermal properties and curing behavior, J. Therm. Anal. Calorim. 111 (2013) 703–710.
[67] E. Savonnet, E. Grau, S. Grelier, B. Defoort, H. Cramail, Divanillin-based epoxy precursors as DGEBA substitutes for biobased epoxy thermosets, ACS Sustain. Chem. Eng. 6 (8) (2018) 11008–11017.
[68] X. Miao, D. Qu, D. Yang, B. Nie, Y. Zhao, H. Fan, Z. Sun, Synthesis of carbon dots with multiple color emission by controlled graphitization and surface functionalization, Adv. Mater. 30 (1) (2018) 1704740.
[69] B.C.M. Martindale, G.A.M. Hutton, C.A. Caputo, S. Prantl, R. Godin, J.R. Durrant, E. Reisner, Enhancing light absorption and charge transfer efficiency in carbon dots through graphitization and core nitrogen doping, Angew Chem. Int. Ed. 129 (23) (2017) 6559–6563.
[70] W. Gu, Z. Dong, A. Zhang, T. Ma, Q. Hu, J. Wei, R. Wang, Functionalization of PET with carbon dots as copolymerizable flame retardants for the excellent smoke suppressants and mechanical properties, Polym. Degrad. Stabil. 195 (2022) 109766.
[71] K.D. Tran, Burn-through resistance of fibre/felt materials for aircraft fuselage insulation blankets, Fire Mater. 26 (1) (2002) 1–6.
[72] R. Ma, R. Shen, Y. Quan, Q. Wang, Tunable flammability studies of graphene quantum dots-based polystyrene nanocomposites using microscale combustion calorimeter, J. Therm. Anal. Calorim. 147 (19) (2022) 10383–10390.
[73] R. Ma, R. Shen, Y. Quan, Q. Wang, Preparation of Graphene Quantum Dots Decorated Montmorillonite to Reinforce Fire Retardancy of Polystyrene, Ind. Eng. Chem. Res. (2023).
[74] L. Zhang, Y. Huang, H. Dong, R. Xu, S. Jiang, Flame-retardant shape memory polyurethane/MXene paper and the application for early fire alarm sensor, Compos. b. Eng. 223 (2021) 109149.
[75] L. Zhang, L. Peng, S. Liang, X. Xie, S. Lyu, S. Wang, Poly (vinyl alcohol)/nanocellulose film integrated with phenolic waste-based carbon dots for ultraviolet-blocking and flame retardant applications, Prog. Org. Coat. 184 (2023) 107872.
[76] R. Jian, P. Wang, W. Duan, J. Wang, X. Zheng, J. Weng, Synthesis of a novel P/N/S-containing flame retardant and its application in epoxy resin: thermal property, flame retardance, and pyrolysis behavior, Ind. Eng. Chem. Res. 55 (44) (2016) 11520–11527.
[77] A. Bifulco, D. Parida, K.A. Salmeia, R. Nazir, S. Lehner, R. Stämpfli, H. Markus, G. Malucelli, F. Branda, S. Gaan, Fire and mechanical properties of DGEBA-based epoxy resin cured with a cycloaliphatic hardener: Combined action of silica, melamine and DOPO-derivative, Mater. Design 193 (2020) 108862.
[78] Z. Sun, Y. Hou, Y. Hu, W. Hu, Effect of additive phosphorus-nitrogen containing flame retardant on char formation and flame retardancy of epoxy resin, Mater. Chem. Phys. 214 (2018) 154–164.
[79] H. Vahabi, F. Laoutid, M. Mehrpouya, M.R. Saeb, P. Dubois, Flame retardant polymer materials: An update and the future for 3D printing developments, Mater. Sci. Eng. R Rep. 144 (2021) 100604.
[80] T. Kashiwagi, F. Du, J.F. Douglas, K.I. Winey, R.H. Harris, J.R. Shields, Nanoparticle networks reduce the flammability of polymer nanocomposites, Nat. Mater. 4 (12) (2005) 928–933.
[81] A. Kausar, Epoxy and quantum dots-based nanocomposites: Achievements and applications, Mater. Res. Innov. 24 (4) (2020) 235–243.

[82] W. Gu, L. Wei, T. Ma, Y. Wu, A. Zhang, J. Wei, R. Wang, Carbon Dots as smoke suppression agents for the reduction of CO release in combustion and improvement of UV resistance towards Phosphorus-containing polyester, Eur. Polym. J. 181 (2022) 111642.
[83] Á. Figueira, L. Oliveira, The current state of fake news: challenges and opportunities, Procedia Comput. Sci. 121 (2017) 817–825.
[84] Y. Sun, X. Le, S. Zhou, T. Chen, Recent progress in smart polymeric gel-based information storage for anti-counterfeiting, Adv. Mater. 34 (41) (2022) 2201262.
[85] B. Yoon, J. Lee, I.S. Park, S. Jeon, J. Lee, J.-M. Kim, Recent functional material based approaches to prevent and detect counterfeiting, J. Mater. Chem. C 1 (13) (2013) 2388–2403.
[86] M. Pan, L. Wang, S. Dou, J. Zhao, H. Xu, B. Wang, L. Zhang, X. Li, L. Pan, Y. Li, Recent advances in colloidal photonic crystal-based anti-counterfeiting materials, Crystals 9 (8) (2019) 417.
[87] H. Qin, S. Zhang, C. Zhao, M. Feng, M. Yang, Z. Shu, S. Yang, Thermal stability and flammability of polypropylene/montmorillonite composites, Polym. Degrad. Stabil. 85 (2) (2004) 807–813.
[88] D. Duraccio, C. Silvestre, M. Pezzuto, S. Cimmino, A. Marra, Polypropylene and polyethylene-based nanocomposites for food packaging applications, in: C. Silvestre, S. Cimmino (Eds.), Ecosustainable Polymer Nanomaterials for Food Packaging, CRC Press, London, 2013, pp. 143–167.
[89] H.A. Maddah, Polypropylene as a promising plastic: A review, Am. J. Polym. Sci 6 (1) (2016) 1–11.
[90] J. Andraos, Safety/hazard indices: Completion of a unified suite of metrics for the assessment of "greenness" for chemical reactions and synthesis plans, Org. Process Res. Dev. 17 (2) (2013) 175–192.
[91] N. Li, Y. Xia, Z. Mao, L. Wang, Y. Guan, A. Zheng, Influence of antimony oxide on flammability of polypropylene/intumescent flame retardant system, Polym. Degrad. Stabil. 97 (9) (2012) 1737–1744.
[92] M.M. Harussani, S.M. Sapuan, U. Rashid, A. Khalina, R.A. Ilyas, Pyrolysis of polypropylene plastic waste into carbonaceous char: Priority of plastic waste management amidst COVID-19 pandemic, Sci. Total Environ. 803 (2022) 149911.